Molecular Therapy
Original Article

A dual-antigen self-amplifying RNA SARS-CoV-2 vaccine induces potent humoral and cellular immune responses and protects against SARS-CoV-2 variants through T cell-mediated immunity

Sean McCafferty,[1,2,9] A.K.M. Ashiqul Haque,[1,9] Aster Vandierendonck,[1] Brian Weidensee,[1] Magalie Plovyt,[1] Magdalena Stuchlíková,[1] Nathalie François,[2] Sophie Valembois,[1] Leo Heyndrickx,[3] Johan Michiels,[3] Kevin K. Ariën,[3,4] Linos Vandekerckhove,[5] Rana Abdelnabi,[6] Caroline S. Foo,[6] Johan Neyts,[6,7] Itishri Sahu,[1,10] and Niek N. Sanders[2,8,10]

[1]Ziphius Vaccines NV, B-9820 Merelbeke, Belgium; [2]Laboratory of Gene Therapy, Department of Veterinary and Biosciences, Faculty of Veterinary Medicine, Ghent University, B-9820 Merelbeke, Belgium; [3]Virology Unit, Department of Biomedical Sciences, Institute of Tropical Medicine, B-2000 Antwerp, Belgium; [4]Department of Biomedical Sciences, University of Antwerp, B-2000 Antwerp, Belgium; [5]HIV Cure and Research Center, Faculty of Medicine and Health Sciences, Ghent University, B-9000 Ghent, Belgium; [6]University of Leuven, Department of Microbiology, Immunology, and Transplantation, Rega Institute for Medical Research, Laboratory of Virology and Chemotherapy, B-3000 Leuven, Belgium; [7]Global Virus Network (GVN), Baltimore, MD, USA; [8]Cancer Research Institute (CRIG), Ghent University, B-9000 Ghent, Belgium

Self-amplifying RNA vaccines may induce equivalent or more potent immune responses at lower doses compared to non-replicating mRNA vaccines via amplified antigen expression. In this paper, we demonstrate that 1 μg of an LNP-formulated dual-antigen self-amplifying RNA vaccine (ZIP1642), encoding both the S-RBD and N antigen, elicits considerably higher neutralizing antibody titers against Wuhan-like Beta B.1.351 and Delta B.1.617.2 SARS-CoV-2 variants compared to those of convalescent patients. In addition, ZIP1642 vaccination in mice expanded both S- and N-specific $CD3^+CD4^+$ and $CD3^+CD8^+$ T cells and caused a Th1 shifted cytokine response. We demonstrate that the induction of such dual antigen-targeted cell-mediated immune response may provide better protection against variants displaying highly mutated Spike proteins, as infectious viral loads of both Wuhan-like and Beta variants were decreased after challenge of ZIP1642 vaccinated hamsters. Supported by these results, we encourage redirecting focus toward the induction of multiple antigen-targeted cell-mediated immunity in addition to neutralizing antibody responses to bypass waning antibody responses and attenuate infectious breakthrough and disease severity of future SARS-CoV-2 variants.

INTRODUCTION

The ongoing pandemic of severe acute respiratory syndrome-coronavirus-2 (SARS-CoV-2) and the associated coronavirus disease 2019 (COVID-19) has caused over 332 million infections as of January 2022.[1] Although the disease commonly causes mild or moderate pulmonary disorder, a substantial proportion of cases progress to severe pneumonia, especially in the elderly and patients with underlying conditions.[2] This has led to the respiratory failure and death of over 5.5 million COVID-19 patients.[1] High human-to-human transmissibility of this virus highlights the importance of the widespread use of safe and effective vaccines that provide the population with the necessary immunity to control this pandemic and decrease COVID-19-related deaths.[3] Only several months after the initial COVID-19 outbreak, messenger ribonucleic acid (mRNA)-based vaccines encoding the SARS-CoV-2 spike (S) glycoprotein were among the first to be approved by regulatory authorities in national immunization programs.[3–5] mRNA vaccines are a novel technology that uses synthetic mRNA molecules, which, after intracellular delivery, instruct cells to produce the antigen(s) that they encode. These vaccines carry many advantages compared to conventional vaccine platforms. First, they allow cell-free production by *in vitro* transcription (IVT), which provides rapid and cost-effective manufacturing, scalability, and flexibility in manipulating antigens of interest. Second, they induce both cellular and humoral immunity due to the intracellular production of antigens and subsequent antigen presentation via both major histocompatibility complex (MHC) class I and II.[6] Although the current authorized mRNA vaccines have demonstrated strong humoral immunogenicity and high short-term efficacy,[7] uncertainty is increasing about the robustness of their protection,[8,9] as

Received 11 February 2022; accepted 18 April 2022;
https://doi.org/10.1016/j.ymthe.2022.04.014.

[9]These authors contributed equally

[10]Senior author

Correspondence: Sean McCafferty, Heidestraat 19 Z03, B-9820 Merelbeke, Belgium.
E-mail: sean.mccafferty@ziphius.org
Correspondence: Itishri Sahu, Heidestraat 19 Z03, B-9820 Merelbeke, Belgium.
E-mail: itishri.sahu@ziphius.org

reports of waning S-antibody levels and evidence of the evasion of neutralizing immunity by several variants of concern (VOC) (especially Beta B.1.351, Delta B.1.617.2, and Omicron B.1.1.529) are emerging.[10–13] To avoid loss of efficacy, periodically updated vaccine boosters that compensate for antibody waning and viral evolution will be needed, especially in high-risk groups.[11,13]

Concomitantly, a growing body of evidence suggests a pivotal role for cell-mediated immunity (CMI) in COVID-19 disease resolution and modulation of disease severity,[14] as waning antibody responses may be compensated for to some extent by CMI responses.[7] Hence, more potent SARS-CoV-2 vaccines can be designed by combining the full-length S or the receptor-binding domain of S (S-RBD) with immunodominant antigens that trigger CMI, such as the membrane (M) or the nucleocapsid (N) proteins.[14,15] Accordingly, we developed ZIP1642, a next-generation self-amplifying RNA (saRNA) vaccine encompassing two different saRNA molecules, that, respectively, encode the S-RBD and the N protein. The saRNA molecules are encapsulated in lipid nanoparticles (LNPs) to protect them from degradation and to facilitate their intracellular delivery into, for example, myocytes and antigen-presenting cells after intramuscular (i.m.) injection.[6] Besides its multi-antigenic character, ZIP1642 has the advantage of having self-replicating features, as the saRNA vaccine encodes a viral RNA replicase in addition to the antigen of interest. Upon cytoplasmic delivery of the saRNA vaccine, the viral replicase is translated and generates multiple copies of the original saRNA vaccine strands. Consequently, a significantly high amount of a shorter subgenomic RNA encoding the antigen is produced.[6] This mechanism leads to high antigen expression levels that can drive equivalent or more potent immune responses at lower doses compared to those achieved by non-replicating mRNA vaccines.[3,6,16]

In this study, the immunogenicity of the dual-antigen saRNA vaccine ZIP1642 and saRNA vaccines encoding either S-RBD or N protein alone was assessed in mice. The vaccines elicited robust antibody responses with high neutralizing antibody titers against the S protein of a Wuhan-like strain, the B.1.351 (Beta) and B.1.617.2 (Delta) variants. Moreover, the saRNA vaccines induced a strong cell-mediated immunity that was characterized by high numbers of S- and N-antigen-specific $CD4^+$ T helper type 1 cell (Th1) and $CD8^+$ T lymphocyte response. Furthermore, prime-boost vaccination with ZIP1642 was able to protect Syrian Golden hamsters (*Mesocricetus auratus*) against a vaccine matching wild-type Wuhan strain-like SARS-CoV-2 as well as a Beta B.1.351 variant. Our findings have important implications for next-generation vaccine development to go beyond the major goal of inducing neutralizing antibodies and additionally aim for multi-antigenic specific T cell responses, which is promising in providing protection against emerging SARS-CoV-2 VOC.

RESULTS

Construction and quality control of SARS-CoV-2 saRNA vaccines

To design our SARS-CoV-2 saRNA vaccines, we optimized the S-RBD and N coding sequences of SARS-CoV-2 for human expression. The linear double stranded (ds) DNA templates were cloned downstream of the subgenomic 5′-UTR of the TC-83 vaccine strain of Venezuelan equine encephalitis virus (VEEV)-derived saRNA sequence,[17] and saRNA constructs were produced via *in vitro* transcription (IVT) (Figure S1). Expression of the SARS-CoV-2 S-RBD or N protein from the individual saRNA vaccine constructs was confirmed via western blot after *in vitro* transfection of mammalian baby hamster kidney (BHK-21) cells (Figure S2). Next, the saRNA constructs were formulated in LNPs containing complexing lipid C12-200, cholesterol, dioleoyl phosphatidylethanolamine (DOPE), and DMG-PEG2000 (Figure S1). For all *in vivo* experiments, LNPs were characterized for size, zeta potential, and saRNA loading (encapsulation percentage) (Table S1). The mean size was ∼110 nm, and the mean charge ranged from −1.2 to +2.5 mV. The encapsulation percentage was consistently ∼97% in all of the *in vivo* studies.

We also assessed the *in vivo* expression potential of our saRNA platform after a first and second injection. In line with the vaccination schedule, mice were injected i.m. with saRNA-LNPs encoding luciferase at days 0 and 21 (Figure 1A). Luciferase expression was subsequently measured via non-invasive *in vivo* imaging (IVIS) over the course of 22 days (Figure S3). Following the first injection, the expression increased rapidly and reached a plateau between days 1 and 8. From day 9 onward, the luciferase expression dropped sharply. After 20 days, the signal became close to background. On day 21, the mice received a second injection. The following day, a luciferase expression similar to that after the first administration was observed (Figure S3).

Immunogenicity of SARS-CoV-2 saRNA vaccines in outbred mice

The immunogenicity of LNP formulations of the S-RBD-saRNA vaccine, the N-saRNA vaccine, and both saRNA vaccines (ZIP1642) was investigated in mice after i.m. vaccination of 1 μg total saRNA according to a prime-boost schedule with a 21-day interval (Figure 1A). The ZIP1642 vaccine contained 0.5 μg of the S-RBD-saRNA and 0.5 μg of the N-saRNA vaccine (1:1 ratio) that were formulated together in a single LNP. As a matched placebo, a group of mice was injected with a mock saRNA vaccine encoding for luciferase (negative control). To measure humoral responses following vaccination, blood was collected 3 weeks post-prime (day 21) and 2 weeks post-boost (day 35). SARS-CoV-2 S1- and N-specific total immunoglobulin G (IgG), IgG1, and IgG2 endpoint titers were determined by ELISA (Figures 1B and S4). Three weeks after priming with the three different saRNA vaccine formulations, all of the mice acquired S1-RBD-specific and N-specific IgG antibodies, while no antibodies were found in the serum of mock vaccinated mice. Administration of a second vaccine dose further increased total IgG endpoint titers, reaching S1-RBD-specific geometric mean titers (GMTs) of 4.71×10^5 and 2.84×10^5, and N-specific GMTs of 8.80×10^4 and 4.80×10^4 for mono-antigenic (S-RBD- or N-saRNA vaccine) and dual-antigenic ZIP1642 vaccine (S-RBD- and N-saRNA vaccine), respectively (Table S2). These data suggest that ZIP1642 is competent in inducing antibody responses against both incorporated antigens, and multi-antigenic immunization does not appear to negatively

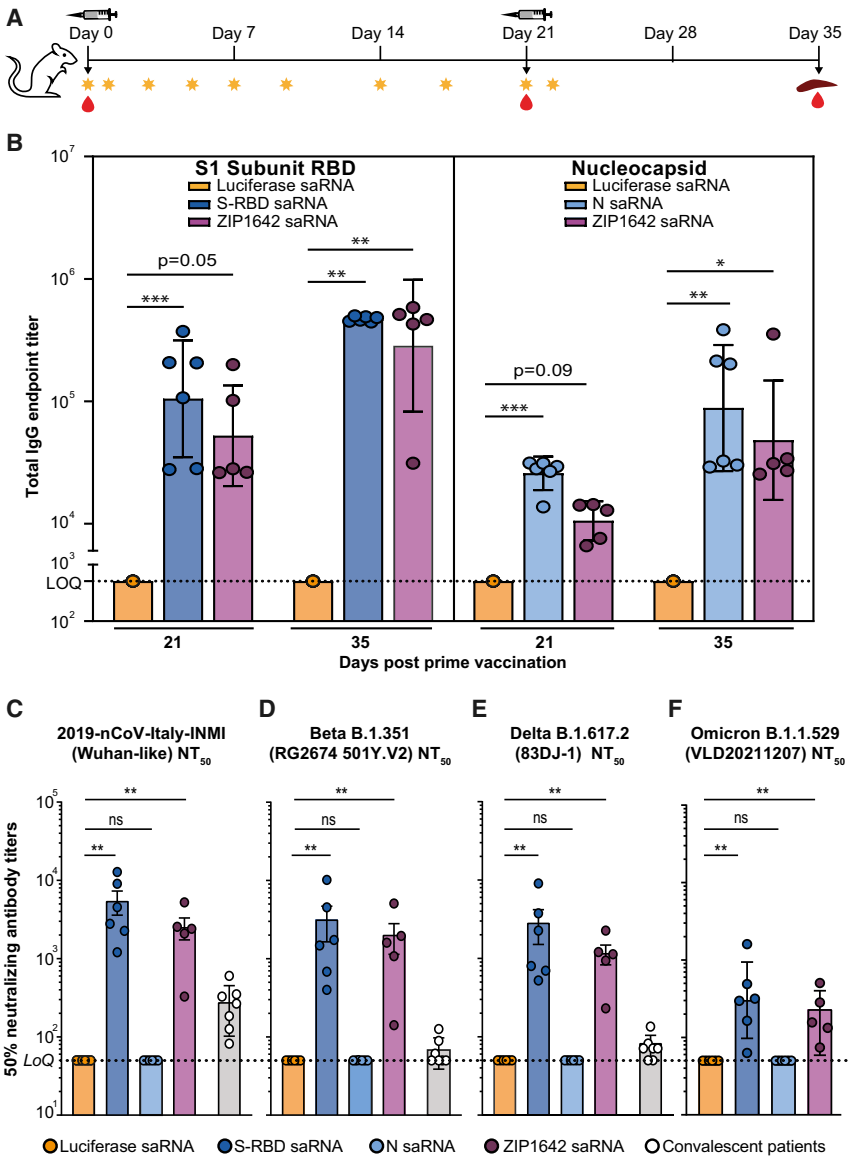

Figure 1. Total IgG antibody titers and SARS-CoV-2 neutralizing titers in Swiss mice vaccinated with dual- or single-antigen saRNA vaccines

Neutralizing titers of COVID-19 convalescent patients were used as reference. (A) Schematic overview of the i.m. vaccination of mice with LNP formulations containing 1 μg S-RBD-saRNA, N-saRNA, or both saRNA species (ZIP1642). ZIP1642 contains 0.5 μg of each saRNA. A prime-boost schedule with 21 days interval was used. Mice vaccinated with a saRNA encoding luciferase were used as control. In these mice, luciferase expression was measured via IVIS over a course of 22 days at indicated time points (orange star). Blood samples were collected just before the prime (day 0), 3 weeks post-prime (day 21), and 2 weeks post-boost (day 35) (red drops). Splenocytes were isolated at day 35 after euthanasia (brown spleen). (B) Serum SARS-CoV-2 S1-RBD and N-specific IgG endpoint titers post-prime (day 21) and post-boost (day 35) vaccination of 6 biologically independent animals. Data are presented as individual datapoints (overlay for luciferase saRNA control) with GMT ± geometric SD; limit of quantification (LOQ) is set at 512. Numerical data can be found in Table S3. (C–F) SARS-CoV-2 wild-type virus neutralization titers (NTs) against 3 variants 2 weeks after boost vaccination of Swiss mice (n = 6) with 1 μg LNP-formulated saRNA vaccines. Serum samples of COVID-19 convalescent patients (n = 7) were included as reference, except for Omicron VNT as no human samples were available at that time. The following 3 SARS-CoV-2 variants were used in the neutralization assays: the Wuhan variant 2019-nCoV-Italy INMI1 (C), the Beta variant 501Y.V2 (D), the Delta variant 83DJ-1 (E), and the Omicron variant VLD20211207 (F). Data are presented as individual datapoints with mean NT_{50} titer ±SD; the limit of quantification (LOQ) is set at 50. Statistical significance of GMTs was determined via a Kruskal-Wallis test, with Dunn's correction for multiple comparisons, and statistical significance of NT_{50} was determined via multiple Mann-Whitney tests. (Adjusted) p values are reported as ns (non-significant); *p < 0.05, **p < 0.01, ***p < 0.001, or ****p < 0.0001.

affect GMT levels compared to mono-antigenic vaccination. Subsequently, we investigated the capacity of the elicited S1-RBD antibodies to neutralize three different SARS-CoV-2 variants: a Wuhan variant (2019-nCoV-Itally INMI1), a Beta variant (501Y.V2), a Delta variant (83DJ-1) and an Omicron variant (VLD20211207) (Figures 1C–1F). Two weeks after boost immunization, all ZIP1642 vaccinated mice showed elevated mean 50% infection reducing neutralization titers (NT_{50}) of 2522, 1971, 1153, and 230 against 2019-nCoV-Italy-INMI1, B.1.351 Beta, B.1.617.2 Delta, and B.1.1.529 Omicron variant, respectively. Mice vaccinated with single-antigen S1-RBD-saRNA vaccine had comparably high neutralizing titers. As expected, the N-saRNA vaccine did not elicit neutralizing titers, as the N-protein is present only inside and not at the surface of SARS-CoV-2. Encouragingly, NT_{50} titers raised by the vaccines were considerably higher than the neutralizing titers found in the sera of convalescent COVID-19 patients (Figures 1C–1E).

Cellular immune responses against more conserved antigens such as the N-protein in our N-saRNA-based vaccines are expected to provide better protection against variants. Therefore, we investigated the T cell responses in mice following vaccination. The amount of antigen-specific interferon-γ (IFN-γ) producing $CD8^+$ and $CD4^+$ T cells in splenocytes was investigated 2 weeks after boost by flow cytometry (Figure 2A; Table S3). Dual-antigen vaccination (ZIP1642) of mice was able to significantly elevate both the S- and N-specific IFN-γ^+ $CD3^+CD4^+$ cell population, reaching mean percentages of 0.077% *(±0.082)* and 0.912% *(±0.644)*, respectively. Similarly, both the S- and N-specific IFN-γ^+ $CD3^+CD8^+$ T cell subsets were also expanded (0.767%

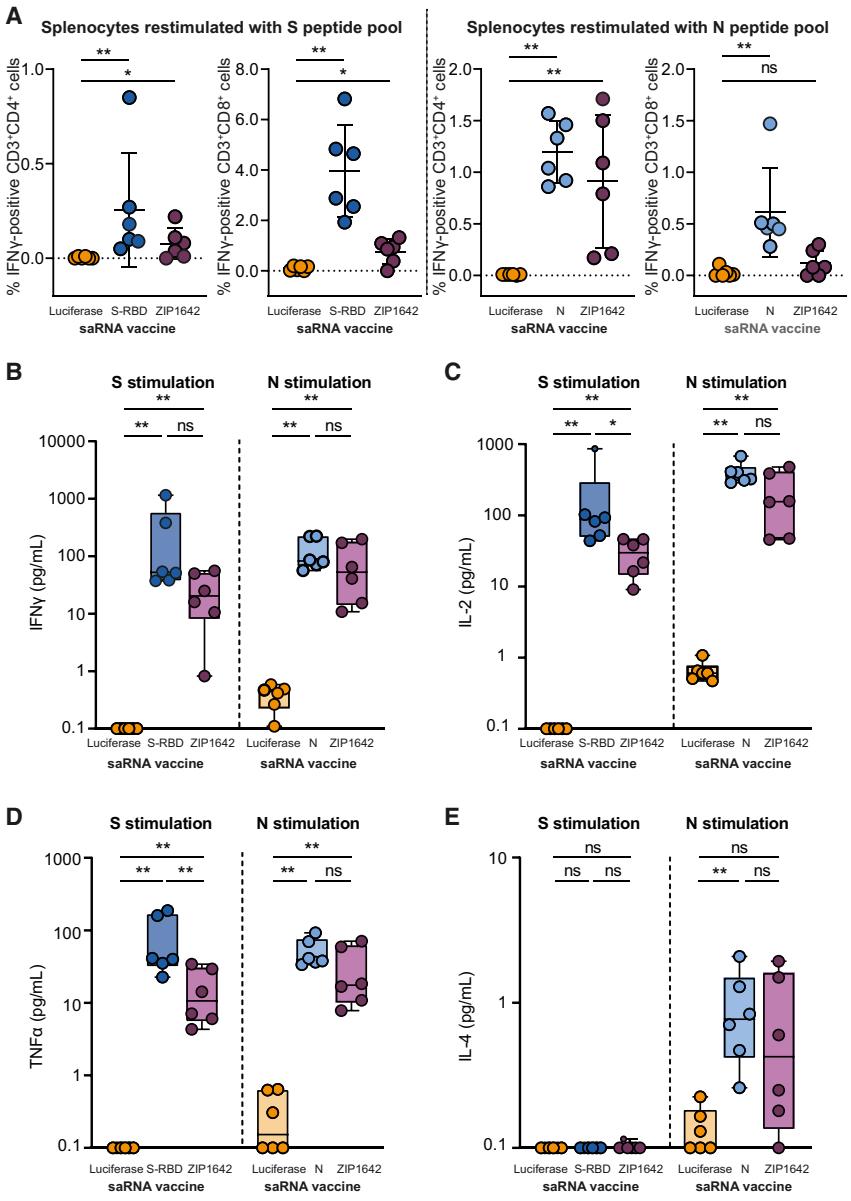

Figure 2. Cellular immune response in Swiss mice after vaccination with dual- or single-antigen saRNA vaccines

(A) Flow cytometric quantification of the percentage of S- or N-specific IFN-γ$^+$ cells in the CD3$^+$CD4$^+$ and CD3$^+$CD8$^+$ splenocyte subpopulations isolated from Swiss mice 2 weeks after booster vaccination with 1 μg S-RBD-saRNA, N-saRNA, or both saRNA vaccines (ZIP1642) (n = 6). Mice injected with a luciferase-encoding saRNA mock vaccine were used as negative controls. Data are presented as individual datapoints, with means ± SDs. Numerical data can be found in Table S3. (B–E) Cytokine release profile from antigen-stimulated splenocytes as measured by a multiplex mouse Th cytokine immunoassay (n = 6). All of the multiplex data are presented as minimum-to-maximum box-and-whiskers plots with median cytokine concentration and lower limit of detection (LLOD) < 0.1. Outliers were determined via the ROUT method (Q = 1%) and presented as small datapoints; outliers were not included in statistical analysis. The asterisks in all of the graphs indicate significance of *p < 0.05, **p < 0.01, ***p < 0.001, or ****p < 0.0001, or ns, as determined by multiple Mann-Whitney tests.

[±*0.486*] and 0.117% [±*0.126*], respectively), but statistical significance could be found only for the S-specific CD8$^+$ T cells. Note that the CD4$^+$ and CD8$^+$ T cell populations induced by ZIP1642 are lower than those elicited upon single antigen vaccination, which may in part be due to the fact that the dose of each individual saRNA construct in ZIP1642 is reduced to half that of the single-antigen vaccines. To further characterize the CMI, we also measured cytokine release from antigen-stimulated splenocytes by a multiplex mouse Th cytokine immunoassay (Figures 2B–2E). We observed that SARS-CoV-2 S restimulated splenocytes from ZIP1642-vaccinated mice yielded increased IFN-γ, interleukin-2 (IL-2), and tumor necrosis factor α (TNF-α) Th1 cytokine secretion, in the absence of Th2 cytokine IL-4 release. Restimulation with a SARS-CoV-2 N peptide pool demonstrated similar results, with an additional increase in Th2 cytokine IL-4 release; however, the latter remained much lower compared to the Th1 cytokines. Prime-boost vaccination with dual-antigen saRNA (ZIP1642) did not cause significant changes in body weight (Figure S5), nor did the mice show clinical signs of adverse effects compared to unvaccinated and luciferase saRNA control groups (data not shown). Collectively, these findings indicate the potential of ZIP1642 in activating SARS-CoV-2-specific CMI, with a Th1-shifted cytokine response.

Low doses of ZIP1642 protect hamsters against WA1/2020 SARS-CoV-2 infection

The protection efficacy of the dual-antigen saRNA vaccine (ZIP1642) against a matching Wuhan strain-like SARS-CoV-2 challenge was investigated in a validated SARS-CoV-2 hamster model.[18,19] Hamsters were immunized following a prime-boost schedule with either 0.1, 1, or 5 μg of the dual-antigen saRNA vaccine. Hamsters that were i.m. injected with 5 μg of a luciferase-encoding saRNA (mock vaccine, negative control) or PBS buffer (sham control) served as negative controls (Figure 3A). Blood was collected before prime (day 0), boost (day 21), and challenge (day 35) to monitor vaccine immunogenicity. Immunization with 0.1 μg ZIP1642 did not lead to a significant induction of S-specific IgG titers. However, doses of 1 and 5 μg induced 100% seroconversion, reaching mean S-specific IgG GMTs of, respectively, 0.72×10^3 and 2.02×10^3 2 weeks after boost (Figures 3B; Table S4). Pseudotyped viruses were used to estimate the capacity of the post-boost elicited antibodies to neutralize a Wuhan strain-like SARS-CoV-2 (D614G mutation). The NT_{50} of hamsters

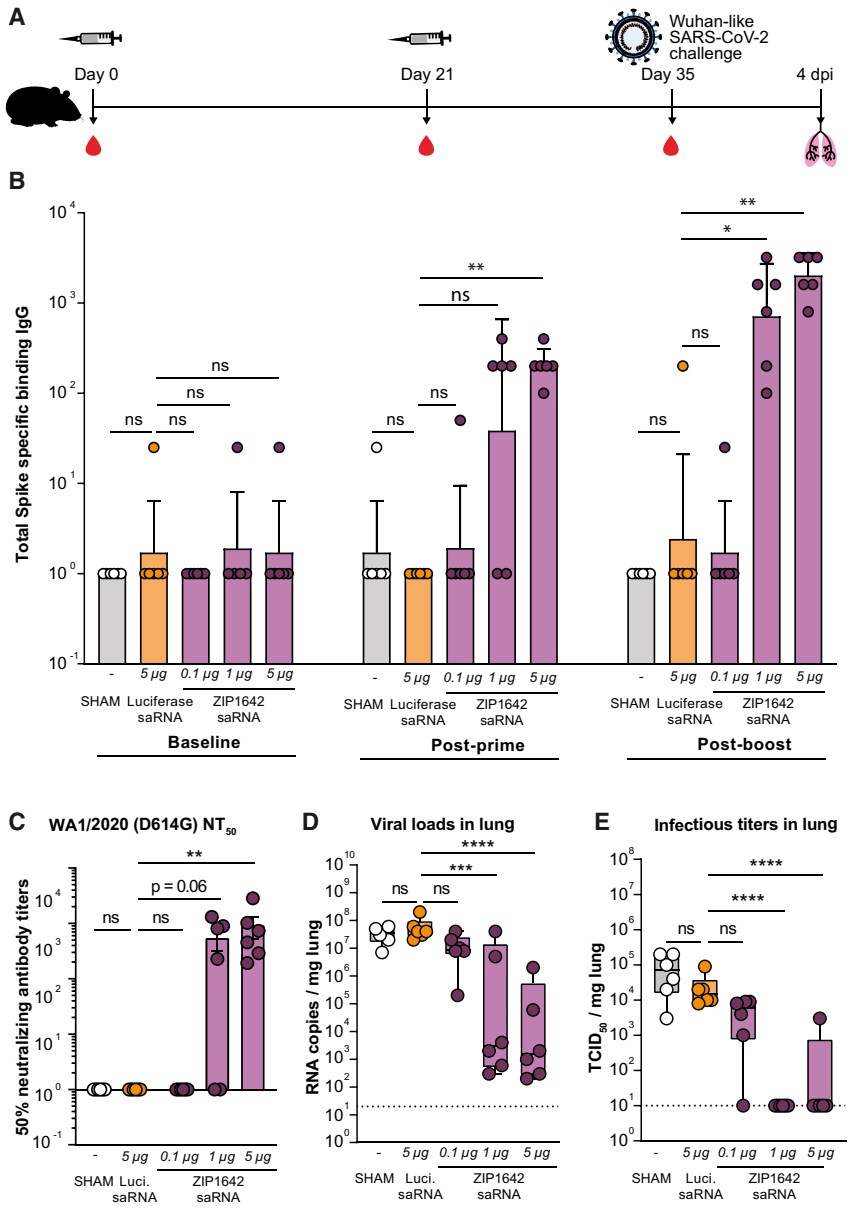

Figure 3. Low doses of the dual-antigen saRNA vaccine ZIP1642 protects Syrian Golden hamsters against WA1/2020 SARS-CoV-2 infection

(A) Schematic overview of i.m. vaccination and intranasal infection of a SARS-CoV-2 Syrian Golden hamster infection model. Female Syrian Golden hamsters (6- to 8-week-old) were vaccinated with 0.1, 1, or 5 μg LNP formulated dual-antigen saRNA vaccine (ZIP1642) following a prime-boost schedule with a 21-day interval. As controls we used hamsters treated with PBS (sham) or 5 μg luciferase saRNA (negative mock control). Blood was sampled at baseline before prime (day 0), before boost (day 21), and 2 weeks post-boost (day 35) (red drops). Two weeks after the booster vaccination, hamsters were intranasally challenged with 1×10^4 $TCID_{50}$ of BetaCov/Belgium/GHB-03021/2020 (EPI ISL 109 407976|2020-02-03), a Wuhan strain-like SARS-CoV-2 virus, that was recovered from a nasopharyngeal swab taken from a qRT-PCR confirmed asymptomatic patient. Lungs were collected after sacrifice, at 4 days post-infection (dpi) (pink lungs). (B) SARS-CoV-2 S-specific IgG end titers at baseline (day 0), post-prime (day 21), and post-boost (day 35) vaccination as determined by IIFA in serum (n = 6). Data are presented as individual datapoints with GMT ± geometric SD. Statistical significance of GMTs was determined via a Kruskal-Wallis testing, with Dunn's correction for multiple comparisons. Numerical data can be found in Table S4. (C) SARS-CoV-2 virus NTs in sera from vaccinated hamsters (n = 6) 2 weeks post-boost (day 35). Neutralization assay was performed using a pseudotyped virus carrying the S of a Wuhan strain-like SARS-CoV-2 (D614G mutation). Data are presented as individual datapoints with mean NT_{50} titer ±SD. Statistical significance of NT_{50} was determined via a Kruskal-Wallis test, with Dunn's correction for multiple comparisons. (D) Viral loads and (E) infectious virus titer ($TCID_{50}$) 4 dpi in homogenized lung tissues as determined by qRT-PCR and endpoint titrations on confluent Vero E6 cells, respectively. Data are presented as minimum-to-maximum box-and-whiskers plots with median reduction of log_{10}-transformed viral RNA load or infectious virus titer per milligram of lung tissue. Statistical significance was determined on log_{10}-transformed data via a 1-way ANOVA with Dunnett's correction for multiple comparisons. A summary of baseline-corrected (relative to sham control) median log_{10}-transformed viral RNA loads and $TCID_{50}$ with corresponding interquartile ranges (IQRs) can be found in Tables S5 and S6. The asterisks in all of the graphs indicate the significance of adjusted $^*p < 0.05$, $^{**}p < 0.01$, $^{***}p < 0.001$, $^{****}p < 0.0001$, or ns, non-significant.

vaccinated with 1 or 5 μg ZIP1642 reached, respectively, 5.40×10^2 and 9.23×10^2, while no NT_{50} titers were observed in the negative controls and in the 0.1-μg ZIP1642 group (Figure 3C). Two weeks after booster vaccination, hamsters were intranasally challenged with a Wuhan strain-like SARS-CoV-2 at 1×10^4 median tissue culture infectious dose ($TCID_{50}$) (Figure 3A). None of the vaccinated animals showed clinical signs of illness before challenge. Vaccination with ZIP1642 led to a non-significant protection of animals from weight loss observed in the negative control groups after viral challenge (Figure S6). Four days after challenge, hamsters were euthanized to detect viral loads and signs of infection in the lungs. High viral loads and infectious virus titers ($TCID_{50}$) were detected in the lungs of sham and mock-vaccinated controls (Figures 3D and 3E), which was associated with severe lung pathology such as bronchopneumonia with apoptotic bodies, peribronchial inflammation, and perivascular inflammation with perivascular cuffs (Figures 4A–4F). These hallmarks resemble pulmonal histopathologic findings in COVID-19 patients with bronchopneumonia. Vaccination with 0.1 μg was not able to significantly reduce viral

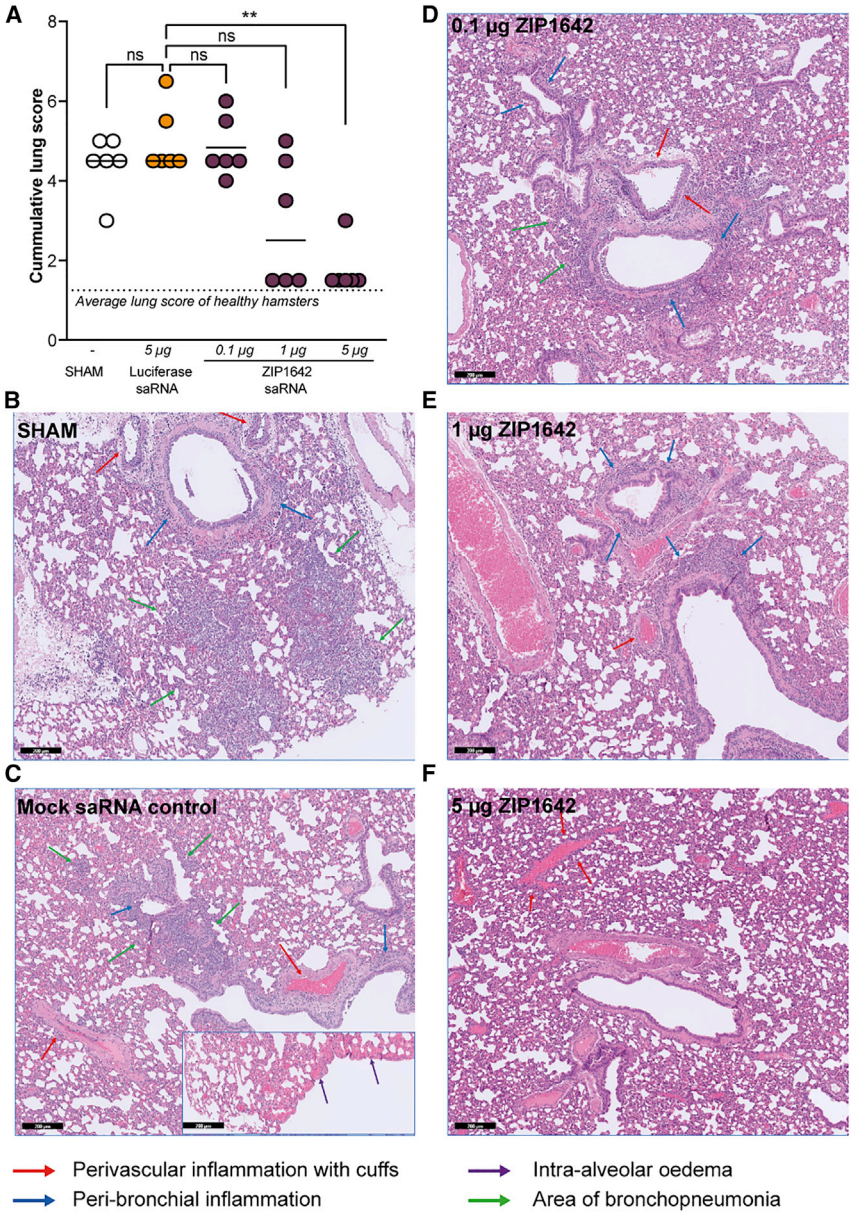

Figure 4. Protection of hamsters against WA1/2020 SARS-CoV-2 infection by ZIP1642 is associated with reduced virus-induced lung pathology

(A) Lung tissue sections were analyzed after H&E staining and scored blindly for lung damage by an expert pathologist. Cumulative lung scores are presented as medians, and the average lung score of healthy hamsters is set at 1.25. The asterisks indicate the significance of *$p < 0.05$, **$p < 0.01$, ***$p < 0.001$, ****$p < 0.0001$, or ns, non-significant, as determined by a Kruskal-Wallis test. (B–F) H&E-stained representative lung tissue sections for each vaccination group (sham, luciferase saRNA mock control, and 0.1, 1, and 5 µg ZIP1642 saRNA). Hallmarks that resemble pulmonal histopathologic findings in COVID-19 patients are indicated, including broncho-pneumonia (green arrows) with apoptotic bodies in the bronchus wall, peribronchial inflammation (blue arrows), perivascular inflammation with perivascular cuffs (red arrows), and intra-alveolar edema (purple arrows). A representative lung tissue section from an untreated healthy hamster can be seen in Figure S7.

load or severe lung pathology. In contrast, 1 and 5 µg of the dual-antigen saRNA vaccine protected hamsters against Wuhan strain-like SARS-CoV-2 infection, with a statistically significant median reduction of 4.0 (interquartile range [IQR] of 0.2–4.9) and 4.4 (IQR of 2.0–5.2) $\log_{10}$-transformed viral RNA load in the lungs, respectively, compared to sham (Figures 3D; Table S5). Accordingly, statistically significant reductions of 3.8 (IQR 3.1–4.3) and 3.4 (IQR 2.3–4.1) $\log_{10}$-transformed $TCID_{50}$ were observed in the lungs of hamsters vaccinated with 1 and 5 µg ZIP1642, respectively, as compared to sham (Figure 3E; Table S6). Furthermore, immunization with 5 µg ZIP1642 significantly reduced virus-induced lung pathology compared to the sham group (Figure 4A) and drastically limited, for example, perivascular inflammation with perivascular cuffs (Figures 4B–4F and S7). Vaccination with 1 and 5 µg ZIP1642 significantly reduced *IP-10* mRNA expression levels, which is an early inflammation marker, in the lungs of challenged hamsters by ~3 $\log_2$-fold compared to both negative control groups (Figure S8). Collectively, these data demonstrate that prime-boost vaccination with a dual-antigen saRNA (ZIP1642) at a dose range of 1–5 µg can elicit adaptive immunity that protects hamsters against Wuhan strain-like SARS-CoV-2 infection and disease.

Immunization with saRNA vaccines encoding Wuhan SARS-CoV-2 nucleocapsid lowers infectious viral load in hamsters challenged with a Beta B.1.351 variant

A second hamster study was conducted to investigate the efficacy of the vaccine against a SARS-CoV-2 variant, and to determine the individual contribution of the S-RBD- and N-saRNA vaccine in the protection efficacy of the dual-antigen vaccine (Figure 5A). We investigated whether the different saRNA vaccines elicited antibodies in hamsters that were able to neutralize SARS-CoV-2 variants. To that end, hamsters were again vaccinated according to a prime-boost schedule with 2 µg of either S-RBD-saRNA, N-saRNA, or dual-antigen saRNA vaccine (ZIP1642). Hamsters injected with 2 µg of a luciferase-encoding saRNA (mock vaccine) served as negative controls. In accordance with the mouse and first hamster challenge study, both the S-RBD-saRNA and dual-antigen saRNA vaccine (ZIP1642) elicited 2-week post-booster Wuhan SARS-CoV-2 S-specific IgG antibodies (indirect immunofluorescence assay [IIFA] assay), with GMTs reaching 1.27×10^3 and 0.72×10^3, respectively (Figure 5B; Table S7). Subsequently, pseudotyped viruses were used

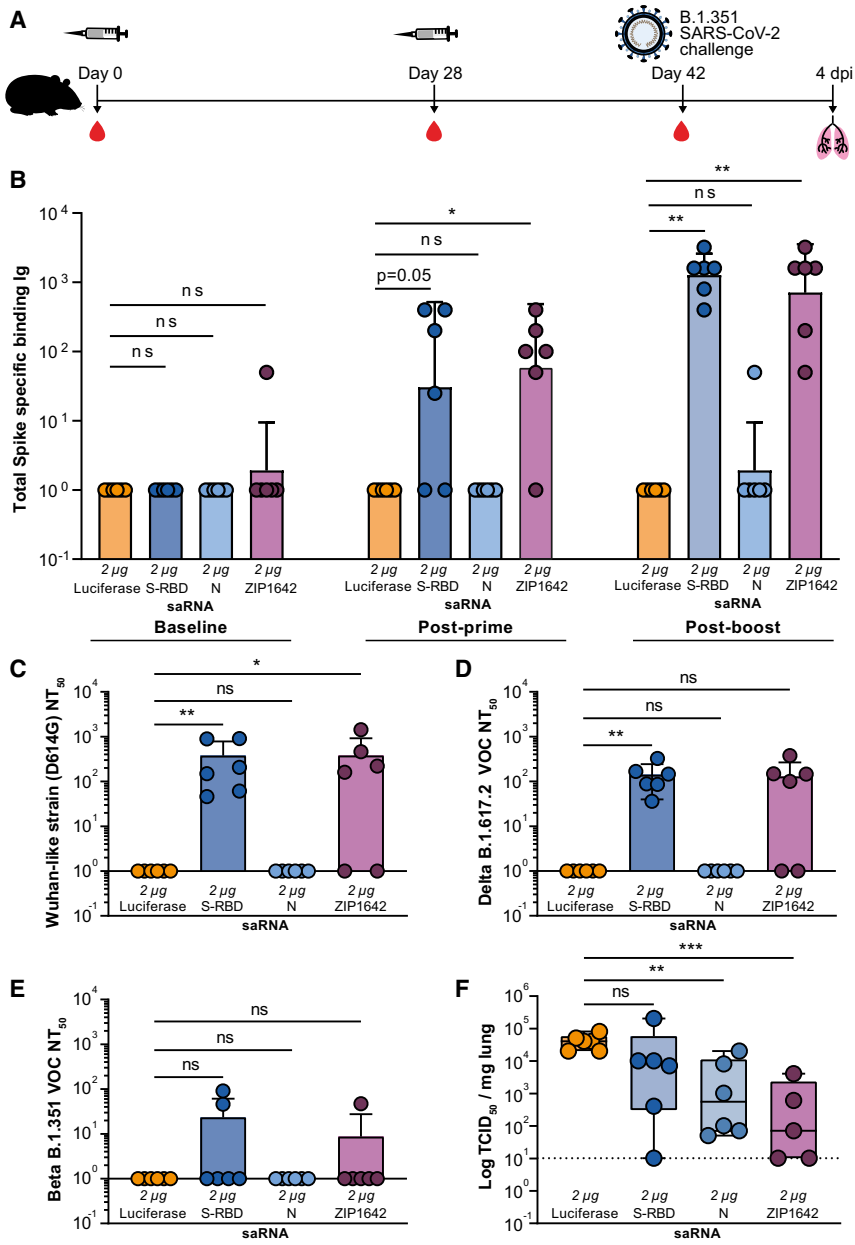

Figure 5. Immunization with saRNA vaccines encoding Wuhan SARS-CoV-2 nucleocapsid lowers viral load in hamster challenged with a SARS-CoV-2 Beta B.1.351 variant

(A) Schematic overview of i.m. vaccination and intranasal infection of a SARS-CoV-2 Syrian Golden hamster infection model. Female Syrian Golden hamsters (6- to 8-week-old) were vaccinated with 2 µg of either S-RBD-saRNA, N-saRNA, or dual-antigen saRNA vaccine (ZIP1642). Hamsters vaccinated with 2 µg of a luciferase encoding saRNA served as negative mock controls. All saRNAs were formulated in LNPs and a prime-boost schedule with a 28 day interval was used. Blood samples were taken before prime (day 0), before boost (day 28), and 2 weeks post-boost (day 42) (red drops). Two weeks after the booster vaccination, hamsters were intranasally challenged with 1×10^4 $TCID_{50}$ of South African variant B.1.351 virus (hCoV-19/Belgium/rega-1920/2021; EPI_ISL_896474, 2021-01-11). Lungs were collected after sacrifice, at 4 dpi (pink lungs). (B) SARS-CoV-2 S-specific IgG end titers at baseline (day 0), post-prime (day 28), and post-boost (day 42) vaccination as determined by IIFA in serum (n = 6 and n = 5 for ZIP1642 group). Data are presented as individual datapoints with GMT ± geometric SD. Statistical significance of GMTs was determined via Kruskal-Wallis testing for multiple comparison. Numerical data can be found in Table S7. (C–E) SARS-CoV-2 pseudotyped virus NTs in sera from vaccinated hamsters two weeks post-boost (n = 6, n = 5 for ZIP1642 group). Neutralization assay was performed using pseudotyped viruses displaying the S protein of respectively (C) Wuhan strain-like SARS-CoV-2 (D614G mutation), (D) Delta B.1.617.2 variant and (E) Beta B.1.351 variant. Data is presented as individual datapoints with mean NT_{50} titer ±SD. Statistical significance of NT_{50} was determined via multiple Mann-Whitney tests. (F) Infectious virus titer ($TCID_{50}$) in lung tissue as determined by endpoint titrations on confluent Vero E6 cells. Data are baseline corrected relative to luciferase saRNA control and presented as minimum-to-maximum box-and-whiskers plots with median reduction of log_{10}-transformed infectious virus titer per milligram of lung tissue. Statistical significance was determined via multiple unpaired t tests on log_{10}-transformed data. A summary of median log_{10}-transformed viral RNA loads and $TCID_{50}$ with corresponding IQRs can be found in Figure S9 and Tables S8 and S9. The asterisks in all of the graphs indicate the significance of adjusted *p < 0.05, **p < 0.01, ***p < 0.001, ****p < 0.0001, or ns, non-significant.

to evaluate whether these anti-S antibodies could neutralize a SARS-CoV-2 Wuhan-like strain (bearing a D614G mutation), as well as the Beta B.1.351 and the Delta B.1.617.2 variants. Neutralization activity against the SARS-CoV-2 Wuhan-like strain was detected in all of the animals vaccinated with 2 µg S-RBD saRNA and 4 of 6 animals vaccinated with the dual-antigen saRNA vaccine, with mean NT_{50}s of 3.76×10^2 and 3.78×10^2, respectively. As expected, no neutralizing titers were observed in negative controls and N-saRNA vaccinated hamsters (Figure 5C). The capacity of the elicited antibodies to neutralize the SARS-CoV-2 Delta variant was 2.5- to 3-fold lower (Figure 5D). Nevertheless, both vaccines raised NT_{50} titers against the Delta variant, which were significantly higher than in the negative control group, with values that equaled 1.42×10^2 and 1.29×10^2, respectively (Figure 5D). Surprisingly, the elicited S-specific antibodies only caused a weak neutralization of the Beta variant, with NT_{50} values that did not reach significance (Figure 5E). These data impelled us to evaluate to what extent a nucleocapsid-based saRNA vaccine, whose protection capacity mostly depends on T cell immunity and non-neutralizing antibody functions, could protect hamsters against a SARS-CoV-2 variant. Therefore, hamsters boosted with the S-RBD-saRNA, N-saRNA, and the dual-antigen saRNA (ZIP1642) vaccine were intranasally challenged with the SARS-CoV-2 Beta B.1.351

variant using 1×10^4 $TCID_{50}$ (Figure 5A). Four days after challenge, the hamsters were euthanized to detect viral loads and signs of infection in the lungs. Hamsters vaccinated with the N-saRNA or dual-antigen saRNA (ZIP1642) vaccine significantly reduced Beta B.1.351 SARS-CoV-2 infection. This was demonstrated by a significant median reduction of 1.0 (IQR of 0.5–1.4) and 1.1 (IQR of 0.7–2.4) log_{10}-transformed viral RNA load in the lungs (Figure S9; Table S8), and 1.8 (IQR 0.7–2.9) and 2.9 (IQR 1.3–3.4) log_{10}-transformed $TCID_{50}$ (Figure 5F; Table S9), respectively, compared to the control group. Nevertheless, virus-induced lung pathology was not significantly improved and no significant changes in IL-6 and inducible protein-10 (IP-10) expression were measured in any of the saRNA-vaccinated groups (Figures S10 and S11). Interestingly, vaccination with the N-saRNA vaccine significantly protected animals from the weight loss that was observed in the negative control group after viral challenge, while the hamsters that were vaccinated with the S-RBD-saRNA vaccine had a body weight decrease similar to that of the negative control group (Figure S12). As expected, based on the *in vitro* neutralizing titer, the S-RBD-saRNA vaccine was not able to protect the hamsters against the Beta variant. Consistent with the previous challenge study, none of the vaccinated animals showed clinical signs of illness before challenge.

Altogether, these data suggest that although prime-boost vaccination with 2 μg S-RBD-saRNA, N-saRNA, or dual-antigen saRNA vaccine (ZIP1642) are not able to significantly induce Spike neutralizing antibody responses against the Beta variant, N-saRNA-containing vaccines are still able to lower the viral load of hamsters challenged with this VOC and to protect the hamster from body weight loss.

DISCUSSION

Before the SARS-CoV-2 pandemic, clinical trials with mRNA-based vaccines mainly focused on non-infectious diseases such as cancer, with only a few trials involving a viral target.[20–23] The battle against the COVID-19 pandemic has proven the enormous potential of mRNA vaccines in accelerating vaccine development through many technical and logistical advantages compared to conventional vaccine platforms.[3] As a result, mRNA-based vaccines were among the first to be authorized for emergency use after the SARS-CoV-2 outbreak.[6]

In this paper, we present an LNP-formulated dual-antigen saRNA vaccine (ZIP1642), consisting of two different saRNAs encoding either the SARS-CoV-2 S-RBD or the N antigen. The self-replicating features of our saRNA vaccines lead to high and prolonged *in vivo* expression of a luciferase reporter antigen. Moreover, we showed that saRNAs can be repeatedly injected without a loss of expression. Importantly, dsRNA by-products that arise during IVT were reduced by cellulose purification, as it has been previously shown to increase vaccine efficiency by reducing the type I IFN response.[24] This approach differs from the one used by Shattock et al. in their preclinical and unsuccessful clinical trial.[25,26]

Recent COVID-19 saRNA vaccine preclinical research[16,26–31] supports the hypothesis that, because of their replicon features, saRNA vaccines are able to induce equivalent or more potent immune responses at lower doses compared to those achieved by non-replicating mRNA vaccines.[3,6] In our study, we confirm this hypothesis and find that multi-antigenic immunization of mice with only 1 μg of the ZIP1642 vaccine was able to induce 100% seroconversion toward high binding GMT values that elicited neutralizing activity against three different SARS-CoV-2 variants (Wuhan, Beta, and Delta variants) that was considerably higher than the neutralizing titers found in the sera of convalescent COVID-19 patients. When comparing with human convalescent sera, one must keep in mind that in preclinical animal studies, sera samples are most often collected shortly after the boost (i.e., at the peak of antibody titers). Our results are consistent with the reports for other saRNA vaccines, in which neutralizing antibody titers against Beta, Delta, and Omicron SARS-CoV-2 variants are reduced compared to those against the Wuhan-like virus.[30] It is important to note that it is challenging to compare our data with other recent preclinical studies that evaluated SARS-CoV-2 saRNA vaccines,[16,26–30] as these vaccination studies are often performed with inbred mice, which have been demonstrated to be immunologically biased and thus have less translational relevance than the outbred mice used in our study. Moreover, these other saRNA vaccine candidates are designed to immunize against the full-length Spike antigen. However, it has been reported that this antigen is not optimal, as the vast majority of the neutralizing response to the SARS-CoV-2 virus is focused on the RBD.[32] Because the RBD has fewer decoy epitopes and thus a greater fraction of the elicited antibodies will be neutralizing, we chose to incorporate this domain as the antigen in our vaccine. Furthermore, the inclusion of fewer epitopes reduces the concern of antibody-dependent enhancement (ADE) induction of RBD-based vaccines, as ADE is primarily mediated through non-neutralizing epitopes. In addition, because of the shorter amino acid sequence of RBD compared to the full Spike, it is much easier to express the RBD protein from the saRNA construct, which may provide a dose-sparing effect. Eventually, shorter sequences will also make it easier to combine several RBD domains of multiple variants into one multivalent vaccine. This is of great value especially for saRNA vaccines, as this platform allows the inclusion of multiple antigens in one replicon using different subgenomic promoters (SGPs), something that is not possible for non-replicating mRNA.

Compared to the majority of other COVID-19 (sa-)mRNA vaccines that are being developed,[4,5,16,26–28,30] the dual-antigen saRNA vaccine ZIP1642 yields the benefit of immunization against two antigens (S-RBD and N SARS-CoV-2 antigen). Reports have been made that the co-transfection of multiple replicon molecules into a single cell may be associated with the impaired translation of one of the constructs, as one RNA species tends to outcompete the other over time.[33,34] Interestingly, we were able to demonstrate similarly high total IgG GMTs and NT_{50}s upon dual-antigen saRNA vaccination with ZIP1642 and upon vaccination with matched single-antigen saRNA vaccines. Note that the single-antigen N-saRNA vaccine cannot elicit neutralizing titers, as the N-protein is not present at the surface of SARS-CoV-2 and hence exerts its effects through cell-mediated immune responses. Altogether, our data indicate that multiple

saRNA transcripts can be delivered in one LNP, with no significant differences in the magnitude of humoral immune responses compared to the single-antigen saRNA vaccines, the latter being consistent with the reports for other COVID-19 saRNA vaccines.[16,26,30]

The rationale for incorporating multiple antigens in one vaccine originates from the growing body of evidence that highlights the necessity of a broad spectrum of immunodominant SARS-CoV-2 proteins to cover the T cell responses required for viral clearance and recovery of COVID-19 patients.[14,35] Hence, a more advanced COVID-19 vaccine design should combine the full-length S or the S-RBD with immunodominant antigens that trigger CMI, such as the M or N proteins.[14] Dual-antigen vaccination of mice with ZIP1642 expanded both the S- and N-specific IFN-γ^+ $CD3^+CD4^+$ and $CD3^+CD8^+$ T cell populations. Murine Th lymphocytes can be defined by their profile of cytokine secretion, meaning the Th1 subset is characterized by its ability to mainly secrete IFN-γ, IL-2, and TNF-α, whereas the Th2 subset primarily produces IL-4. Dual-antigen vaccination of mice with ZIP1642 suggests a IFN-γ^+/IL-2^+/TNF-α^+ Th1 shifted and slightly more balanced IFN-γ^+/IL-2^+/TNF-α^+/IL-4^+ cytokine response of splenocytes upon S- and N-protein restimulation, respectively. Similarly, the N-specific serum IgG2a:IgG1 immunoglobulin isotype ratio, an indicator of Th1/Th2 lymphocyte dominance in rodents, of ZIP1642 vaccinated mice is slightly more balanced than the Th1 skewed S-specific IgG2a:IgG1 ratio. It is important to note that the T cell responses induced by ZIP1642 are lower than those elicited upon single-antigen vaccination. This may be due to the fact that the dose of each individual saRNA construct in ZIP1642 is reduced to half that of the single-antigen vaccines. However, our CMI data do not allow us to fully exclude any possibility of replicating competition due to co-transfection of multiple replicon molecules into a single cell or antigenic interference.[36]

We hypothesized that cellular immune responses against more conserved antigens such as the N-protein in our N-saRNA-based vaccines should provide better protection against variants displaying highly mutated Spike proteins, as antibody responses may be compensated to some extent by CMI responses.[7] Accordingly, we evaluated this hypothesis by challenging vaccinated hamsters with either Wuhan strain-like SARS-CoV-2 or the Beta B.1.617.2 variant. A dose of 1 μg of ZIP1642 was found to effectively clear infectious Wuhan strain-like SARS-CoV-2 titers ($TCID_{50}$) in all hamsters, while NT_{50} values against this strain were zero in two animals, suggesting a pivotal role for T cell immunity, or potentially non-neutralizing antibody functions, for viral clearance in the two hamsters that did not elicit neutralizing antibodies at this low dose. Moreover, the vaccination of hamsters with the dual-antigen saRNA vaccine only elicited elevated neutralizing antibody responses against the antigen-matched Wuhan-like strain, and a very weak, non-significant neutralization against the Beta variant, while the dual-antigen saRNA vaccines significantly decreased viral loads of both variants after challenge. The low NT_{50} against the Beta variant is somehow unexpected, but is in line with the work of Maruggi et al., who also found lower NTs against this variant after vaccination with a saRNA vaccine encoding full-length S of Wuhan SARS-CoV-2.[30] In addition, we demonstrated that mono-antigenic S-RBD vaccination is not able to clear Beta SARS-CoV-2 viral loads. Altogether, our data confirm that the protection capacity of our dual-antigen saRNA vaccine ZIP1642 in this infection model depends on T cell-mediated responses or potentially non-neutralizing antibody functions against the N-protein. Note that the protection capacity of the single-antigen S-RBD-saRNA vaccine against the wild-type and SARS-CoV-2 Delta variant was not determined in our studies, as our focus was on the dual-antigen vaccine. Nevertheless, the viral NTs, which are a reliable indicator of protection, show very good and moderate protection against the wild-type and Delta variant, respectively.

The absence of a significant reduction in Beta virus-induced lung pathology in the vaccinated hamsters compared to the control groups could be explained by the lower clearance of the Beta variant (only 2 of 6 ZIP1642 vaccinated hamsters had undetectable infectious Beta viral titers). It is possible that in an experimental setup with prolonged post-infection time (>4 days post-infection [dpi]), reduction in lung tissue damage may be observed as the CMI needs more time to reduce infectious B.1.617.2 viral titers toward full clearance. Note that both the Wuhan strain-like and Beta variant pulmonary viral loads are less reduced than the infectious viral titers ($TCID_{50}$), which may be due to the ability of qRT-PCR to also pick up inactivated or dead viruses.

Nonetheless, our data suggest that protection against VOCs may be possible by bypassing waning antibody responses via cellular immunity or non-neutralizing antibody functions, especially when targeting multiple viral antigens to evoke a broader T cell response. These results are consistent with the expanding number of reports highlighting the importance of CMI and its contribution to protection when antibody titers are borderline or subprotective in patients.[7,14,37–39] Importantly, these findings may be of particular value in addressing the issue of variable loss of antibody potency induced by the current authorized SARS-CoV-2 vaccines against the newly emerged Omicron VOC, as the World Health Organization (WHO) recently reported that cellular immunity may be more preserved than neutralizing antibody responses against this highly mutated variant.[39] Thus far, booster shots of the current authorized vaccines have been advised and approved to increase protection against new SARS-CoV-2 VOCs by efficiently restoring high neutralizing titers, as regulatory authorities consider neutralization to be the leading correlate of protection from viral infection.[11,39] However, supported by the results of this study, we encourage the concept of redirecting focus toward the induction of CMI and non-neutralizing vaccine-elicited antibody-mediated functions against multiple antigens in addition to targeting neutralizing antibody responses, to attenuate infectious breakthrough and disease severity. It is important to note that although not investigated in this study, other vaccine-elicited antibody-mediated functions (e.g., antibody-dependent cellular phagocytosis) and natural killer (NK) CMI responses should also be considered as these also contribute to disease protection. In addition, the longevity and memory capacity of the established immune responses of ZIP1642 should be considered in future studies.

In conclusion, our results advocate that further accelerating the development of new multi-antigenic vaccines, such as the ZIP1642 saRNA vaccine, should be considered to yield greater protection against emerging and potential future SARS-CoV-2 variants or other viruses.

MATERIALS AND METHODS

Vaccine construct design and production

Plasmids containing the IVT template flanked by I-SceI restriction sites were high-copy plasmids containing the β-lactamase (bla) resistance gene. The IVT template consisted of a T7 RNA polymerase promoter followed by the desired saRNA sequence. The encoded saRNA sequence is derived from the TC-83 vaccine strain of VEEV but contains an A3>G substitution and the nsP2 Q739L non-cytopathic mutation.[17] The S-RBD (derived from full-length Spike GenBank: YP_009724390.1) and N protein (GenBank: YP_009724397.2) coding sequences were optimized for human expression using the GeneOptimizer algorithm and ordered as linear dsDNA with appropriate overlaps (GeneArt; Thermo Fisher Scientific, Regensburg, Germany) for homology-based cloning (HiFi DNA Assembly, New England Biolabs, Ipswich, MA, USA) downstream of the subgenomic 5′-UTR. Cloning reactions were transformed via heat shock into *Escherichia coli* cells (NEB 5-alpha Competent *E. coli* High Efficiency, C2987H; New England Biolabs). Plasmid DNA was isolated using the Qiagen Plasmid Plus Midi Kit (12945; Qiagen, Hilden, Germany), and sequences were verified using the Sanger method. Plasmids were digested using I-SceI (R0694S; New England Biolabs), and an analytical amount was loaded on an agarose gel for digest verification. Plasmid digests were purified via silica spin columns (Wizard SV gel and PCR Clean-up System A9285; Promega, Madison, WI, USA). Linearized plasmid DNA was used as a template for the IVT reaction via the HiScribe T7 High Yield RNA Synthesis Kit (E2040S; New England Biolabs), with co-transcriptional capping using CleanCap technology (CleanCap AU N711410; Trilink BioTechnology, San Diego, CA, USA), following the manufacturer's instructions. Briefly, DNA samples were supplemented with unmodified ribonucleotide solutions, MEGAscript reagents, and CleanCap AU, and incubated for 2–3 h at 37°C. IVT saRNA samples were treated with 2 U/μL turbo DNase for 15 min at 37°C to remove template DNA. For IVT saRNA cleanup, samples were mixed with RNA Cleanup Binding Buffer and ethanol (>95%, EtOH) and transferred on silica-based spin columns (T2050L; Monarch CleanUp Kit, New England Biolabs). The saRNA concentration was determined using Nanodrop. IVT saRNA samples were purified using cellulose (11365; Avicel PH-101 microcrystalline cellulose, Sigma-Aldrich, St. Louis, MO, USA) to reduce the dsRNA content.[24,40] In short, saRNA was mixed with 0.2 g cellulose/mL 16% EtOH-HEPES chromatography buffer and shaken for 30 min. Samples were spun down at room temperature (RT) (14,000 × *g*, 1 min, 20°C) and mixed with prewashed cellulose for a second time. After centrifugation (14,000 × *g*, 1 min, RT), the ss saRNA was mixed with sodium acetate (NaOAc, pH 5.5) and 1 volume of isopropanol for precipitation, and chilled at −20°C for 30 min before centrifugation (14,000 × *g*, 15 min, 4°C). The resulting pellet was washed with 70% EtOH and resuspended in RNase-free water after an additional centrifugation step (14,000 × *g*, 10 min, 4°C). RNA purity, size, and concentration was determined via fragment analysis (Agilent RNA Kit, Agilent [Santa Clara, CA, USA], 15 nt, DNF-471-0500; with 50 μg 50575 Lonza RNA marker). The purified saRNA was dissolved in nuclease-free water and stored at −80°C until further use.

Confirmation of *in vitro* antigen expression of saRNA constructs

Transfection of mammalian baby hamster kidney cells

BHK-21 [C13] cells (CCL10, ATCC, Manassas, VA, USA) were transfected using the Lipofectamine MessengerMAX mRNA transfection protocol (Thermo Fisher Scientific, Waltham, MA, USA). In brief, BHK-21 cells were cultured in Eagle's minimum essential medium (EMEM), supplemented with 10% fetal bovine serum (FBS), and sub-cultivated at a 1:2–1:10 ratio. Cells were seeded in 24-well plates at a 50,000 cells/well density to be 70%–90% confluent and washed with Dulbecco's phosphate-buffered saline (DPBS). Cells were transfected according to the manufacturer's guidelines by diluting and incubating the MessengerMAX Reagent in Opti-MEM medium for 10 min at RT. saRNA samples and controls encoding for enhanced green fluorescent protein (EGFP) were diluted in OptiMEM medium as well, and incubated for 5 min at RT with diluted MessengerMAX reagent in a 1:1 ratio. The BHK-21 cells were incubated with this mixture for 24 h at 37°C/7% CO^2. Transfection was confirmed by EGFP visualization using fluorescence microscopy.

Antigen protein isolation from BHK-21 cells

Transfected BHK-21 cells were collected following trypsinization (3–5 min) and centrifugation (300 × *g*, 5 min, RT), and total protein cell lysates were collected (10,000 × *g*, 10 min, RT) after homogenization with Tissue Extraction Reagent I (Thermo Fisher Scientific) Tris-based lysis buffer supplemented with Halt protease inhibitor cocktail (1X) (78,429, Thermo Fisher Scientific).

Western blot

Total protein cell lysates were mixed with lithium dodecyl sulfate (LDS) sample buffer, sample reducing agent, and double-distilled water (ddH_2O), heated at 70°C for 10 min and loaded on NuPAGE Bis-Tris gels (100 V, 1 h). To detect saRNA-mediated protein expression, samples were electrophoretically transferred to a nitrocellulose membrane by western blotting (30 V, 1 h). The membrane was blocked with milk and incubated overnight at 4°C with polyclonal rabbit antibody against SARS-CoV-2 S protein S1 RBD (1:1,000, #130-10759, RayBiotech, Peachtree Corners, GA, USA) and polyclonal rabbit antibody against SARS-CoV-2 N protein (1:1,000, #130-10760, RayBiotech). goat anti-rabbit IgG-horseradish peroxidase (HRP)-conjugated secondary antibody (168-11090, RayBiotech) (1:20,000, 45 min, RT) and 3,3′, 5,5′ tetramethylbenzidine dihydrochloride (TMB) substrate were used to allow protein band visualization.

LNP formulation and characterization

Microfluidic mixing

saRNA constructs were formulated in LNPs on the Ignite NxGen System (Precision Nanosystems, Vancouver, BC, Canada), by mixing 1 volume of a lipid solution (in 100% EtOH) and 3 volumes of saRNA (1:3 ratio) in citrate buffer (pH 3, 10 mM). The lipid solution was

prepared by dissolving individual lipids in 100% EtOH at a total concentration of 1.5 mg/mL consisting of 35 mol % complexing lipid (C12-200, LP-04-425, CordenPharma, Brussels, Belgium), 43.5 mol % cholesterol (plant powder, 700100P; Sigma-Aldrich), 20 mol % 1,2-di-(9Z-octadecenoyl)-*sn*-glycero-3-phosphoethanolamine (DOPE) (850725P; Sigma-Aldrich), and 1.5 mol % 1,2-dimyristoyl-rac-glycero-3-methoxypolyethylene glycol-2000 (DMG-PEG2000) (880151P; Sigma-Aldrich). The ratio of complexing lipid to saRNA was maintained at an N:P ratio of 37:1. The flow rate was set at 12 mL/min and a NxGen single-use cartridge (Precision Nanosystems) was used for Y-tubing-based microfluidic mixing (Precision Nanosystems).

Ribogreen assay (concentration)

The saRNA loading in LNP formulations was quantified using a Quant-iT RiboGreen assay (Thermo Fisher Scientific) as previously described.[41] Samples were diluted 10-fold in 1× Tris-EDTA (TE) buffer with or without 0.5% (v/v) Triton X-100 (Sigma-Aldrich). Standard solutions were also prepared in 1× TE with or without 0.5% (v/v) Triton X-100 to account for any variation in fluorescence. The assay was performed according to the manufacturer's protocol. Samples were loaded on a black 96-well plate and analyzed for fluorescence on a microplate reader (Tecan Infinite 200 PRO) at an excitation of 485 nm and emission at 528 nm. *In vitro* and *in vivo* dosing was defined based on the calculated encapsulated dose.

Zeta potential (charge)

The zeta potential of LNPs was assessed with using the ZetaSizer Nano ZS90 (Malvern Panalytical, Westborough, MA, USA). LNP suspension was diluted 1/10 in PBS, equilibrated at RT, and analyzed in a disposable folded capillary cell using the following settings: dispersant viscosity of 0.882 cP, refractive index of 1.33, and dielectric constant of 79.

Size

Analyses were performed by NanoSight NS300 instruments (Malvern Instruments, Malvern, UK). The instruments were equipped with a 488-nm laser, a high-sensitivity sCMOS camera, and a syringe pump. The LNP suspension was diluted in particle-free PBS (0.02 μm filtered) to obtain a concentration within the recommended measurement range ($1–10 \times 10^8$ particles/mL), corresponding to dilutions from 1:100 to 1:100,000, depending on the initial sample concentration. Experiment videos were analyzed using Nanoparticle Tracking Analysis (NTA) software (Malvern Instruments) after capture in script control mode (5 videos of 60 s per measurement) using syringe pump speed 50. A total of 1,500 frames were examined per sample to determine the LNP size.

Animal immunization and viral challenge

For the immunization study, female Swiss mice (6–8 weeks old) were purchased from Janvier Laboratories (Paris, France) and kept in individually ventilated cages with access to food and water *ad libitum*. Mice experiments were approved by the ethics committee of the Faculty of Veterinary Medicine, Ghent University (EC no. EC2020/043). Mice were anesthetized with isoflurane (Zoetis, Louvain-La-Neuve, Belgium) (5% for induction and 2% for maintenance) and i.m. injected with a total of 1 μg in 100 μL DPBS (50 μL per leg) LNP-formulated saRNA (S-RBD saRNA, N saRNA), or a 1:1 mass ratio of co-formulated S-RBD and N saRNA (0.5 μg S-RBD saRNA and 0.5 μg N saRNA), or luciferase saRNA as negative mock control; for each group, n = 6). All of the groups were immunized according to a prime-boost injection regime with a 21-day interval. Negative control groups were analyzed for luciferase-induced bioluminescence via non-invasive *in vivo* bioluminescent imaging (IVIS Lumina III, PerkinElmer, Waltham, MA, USA), 12 min after subcutaneous injection of 100 μL of D-luciferin (GoldBio, #LUCK-1G, St. Louis, MO, USA). Retro-orbital blood sampling was performed before prime (day 0) and boost (day 21) and at sacrifice (day 35). Mice were euthanized after sedation with isoflurane via cervical dislocation. Spleens were harvested and serum was collected post-blood coagulation by centrifugation (2,000 × *g*, 15 min, 4°C) and stored (−80°C) until use.

KU Leuven Rega Institute (Leuven, Belgium) has developed and validated a SARS-CoV-2 Syrian Golden hamster infection model.[18,19] For the evaluation of the potential antiviral activity of our vaccines, two wild-type SARS-CoV-2 challenge studies in hamsters were performed. Live virus-related work was conducted in the high-containment A3 and BSL3+ facilities of the KU Leuven Rega Institute (3CAPS) under licenses AMV 30112018 SBB 219 2018 0892 and AMV 23102017 SBB 219 20170589, according to institutional guidelines. Six- to 8-week-old female wild-type Syrian Golden hamsters were purchased from Janvier Laboratories (Paris, France) and were housed as pairs in ventilated isolator cages (IsoCage N Biocontainment System, Tecniplast, Fisher Scientific) with *ad libitum* access to food and water and cage enrichment (wood block). The animals were acclimated for 4 days before the start of the study. Housing conditions and experimental procedures were approved by the ethics committee of animal experimentation of KU Leuven (license P065-2020). Hamsters were anesthetized with ketamine/xylazine/atropine before i.m. immunization in a total vaccine volume of 200 μL (100 μL in each leg). In an initial study, the animals were injected according to prime-boost regimen with a 21-day interval with either sham (PBS), 5 μg of luciferase saRNA (negative mock control), or 0.1, 1, or 5 μg of ZIP1642 saRNA. In a second study, animals were injected according to prime-boost regimen with a 28-day interval with either 2 μg luciferase saRNA (negative mock control), 2 μg S-RBD saRNA, 2 μg N saRNA, or 2 μg ZIP1642 saRNA. Groups of both studies comprised 6 animals (n = 6), and blood was sampled via the jugular vein at baseline before prime, before boost, and 2 weeks post-boost. Subsequently, 2 weeks post-boost, animals were challenged intranasally with 50 μL medium containing 2% FBS (~25 μL/nare), containing 1×10^4 $TCID_{50}$ SARS-CoV-2. For the first challenge study, BetaCov/Belgium/GHB-03021/2020 (EPI ISL 109 407976|2020-02-03) was recovered from a nasopharyngeal swab taken from a qRT-PCR-confirmed asymptomatic patient who returned from Wuhan, China at the beginning of February 2020; a close relation with the prototypic Wuhan-Hu-1 2019-nCoV (GenBank accession 112: MN908947.3) strain was confirmed by phylogenetic analysis. For the second challenge study, South African variant

B.1.351 virus (hCoV-19/Belgium/rega-1920/2021; EPI_ISL_896474, 2021-01-11), was recovered from a nasopharyngeal swab taken from a patient returning to Belgium in January 2021 with respiratory symptoms. The strain was subjected to sequencing on a MinION platform (Oxford Nanopore, Didcot, UK) directly from the nasopharyngeal swabs. For both studies, infectious virus was isolated by serial passaging on Vero E6 cells; passage 3 and 2 virus was used for the first and second study, respectively. The titers of both virus stocks were determined by endpoint dilution on Vero E6 cells by the Reed-Muench method.[42] From challenge onward, the hamsters were weighed daily and observed for mobility, self-maintenance, behavior, and humane endpoint (hindlimb paralysis, hunchback, souring of eyes). At 4 dpi, hamsters were euthanized by intraperitoneal injection of 500 μL Dolethal (200 mg/mL sodium pentobarbital, Vétoquinol SA, Lure, France). Blood and lungs were collected at endpoint. Serum was isolated post-blood coagulation by centrifugation (10,000 × *g*, 10 min, RT) and stored frozen at −80°C until use.

Analysis of humoral immune response

Convalescent serum samples of cured COVID-19 patients

Serum samples of non-hospitalized cured COVID-19 patients were obtained with informed consent. The recruitment and sampling procedures were approved by the ethics committee (no. BC-08071). Human COVID-19 convalescent sera (n = 7) were obtained from donors 41–75 years of age (5 females, 2 males) at least 30 days–8 months post-infection. The presence of anti-SARS-CoV-2 antibodies in all of the obtained sera was confirmed using a SARS-CoV-2 Surrogate Virus Neutralization Test Kit (#L00847, GenScript, Piscataway, NJ, USA). All of the human sera were obtained from the Ghent University Hospital (Ghent, Belgium).

Detection of mouse binding antibodies by antigen-specific IgG ELISA

To assess antigen-specific total IgG titers in mouse sera, Nunc MaxiSorp 96-well plates (# 44-2404-21, Thermo Fisher Scientific) were coated overnight at 4°C with 1 μg/mL recombinant SARS-CoV-2 S1 subunit protein RBD (rSARS-CoV-2 S-RBD, #230-30162-500, RayBiotech) or 500 ng/mL recombinant SARS-CoV-2 N protein (rSARS-CoV-2 N, #230-30164-500, RayBiotech). rSARS-CoV-2 S-RBD was dissolved in PBS-based coating buffer (pH 7.2), while rSARS-CoV-2 N was dissolved in carbonate coating buffer (pH 9.6), determined upon *in silico* prediction of the isoelectric points (pH(I)) of the coating proteins (pH(I) = 5.4 and 9.4, respectively). After washing 4 times with 200 μL/well PBS with 0.05% Tween-20, ELISA plates were blocked with 2× Assay Buffer (from IgG Total Mouse Uncoated ELISA Kit, #88-50400-86, Thermo Fisher Scientific) for 2 h at RT. Following blocking and 4 washes, serum samples prediluted in 1X assay buffer and HRP-conjugated detection antibodies for IgG total (1:250, polyclonal anti-mouse IgG detection antibody from the IgG Total Mouse Uncoated ELISA Kit, #88-50400-86, Thermo Fisher Scientific), IgG1 (1:40,000, polyclonal goat anti-mouse IgG1 HRP, #ab97240, Abcam, Cambridge, UK) and IgG2a (1:5,000, polyclonal goat anti-mouse IgG2a secondary antibody [HRP], #M32207, Thermo Fisher Scientific), respectively, were co-incubated in the antigen-coated plates on a shaker set at 400 rpm for 2 h at RT. Plates were washed 7 times and treated with 100 μL/well TMB substrate solution (from the IgG Total Mouse Uncoated ELISA Kit, #88-50400-86, Thermo Fisher Scientific). After 10 min, 2 N H_2SO_4 was added to stop the reaction, and the absorbance was read on a spectrophotometer at 450 nm.

Detection of hamster binding antibodies by IIFA

To detect specific antibodies to SARS-CoV-2 S protein in hamster serum, an IIFA developed at the University of Leuven was used. Using CRISPR-Cas9, a CMV-SARS-CoV-2-Spike-FLAG-IRES-mCherry-P2A-BlastiR cassette was stably integrated into the ROSA26 safe harbor locus of HEK-293T cells.[43] To determine SARS-CoV-2 Spike binding antibody end titers, 1/2 serial serum dilutions were made in 96-well plates on HEK-293T Spike stable cells and HEK-293T wild-type cells in parallel. Goat anti-hamster IgG(H + L)-fluorescein isothiocyanate (FITC) (1:250 diluted; SouthernBiotech, Birmingham, AL, USA) was used as the secondary antibody. After counterstaining with DAPI, fluorescence in the blue channel (excitation at 386 nm) and the green channel (excitation at 485 nm) was measured with a Cell Insight CX5 High Content Screening platform (Thermo Fisher Scientific). Specific SARS-CoV-2 Spike staining is characterized by cytoplasmic (endoplasmic reticulum [ER]) enrichment in the green channel. To quantify this specific SARS-CoV-2 Spike staining, the difference in cytoplasmic and nuclear signal for the HEK-293T wild-type conditions (background) was subtracted from the difference in cytoplasmic and nuclear signal for the HEK-293T Spike stable cells. All of the positive values were considered to be a specific SARS-CoV-2 Spike binding signal. The IIFA end titer of a sample is defined as the highest dilution that scored positive in this way.

Wild-type viral neutralization assay (VNT) for mouse serum

Wild-type VNT with mouse serum samples and convalescent human patient serum samples was performed by the Institute of Tropical Medicine (Antwerp, Belgium) as previously described.[44,45] Serum dilutions in medium were incubated with 3 × $TCID_{100}$ of SARS-CoV-2 variants (2019-nCoV-Italy-INMI1 with close relation with the prototypic Wuhan-Hu-1 2019-nCoV, RG2674 B.1.351 Beta variant 501Y.V2, and 83DJ-1 Delta variant B.1.617.2) during 1 h at 37°C/7% CO_2. Subsequently, 8 × 100 μL of the sample virus mixtures were added to 100 μL cell suspension containing 18,000 Vero cells in the wells of a 96-well plate and incubated for 5 days in a humid incubator at 37°C/7% CO_2. The cytopathic effect (CPE) of each well was evaluated and scored microscopically as negative or positive for viral growth. The Reed-Muench method[42] was used to calculate the NT that reduced the number of infected wells by 50% (NT_{50}), with a lower limit of quantification (LOQ) of 50.

Pseudotyped viral serum neutralization test

SARS-CoV-2 Spike protein neutralizing antibody (nAb) titers were determined using Spike-pseudotyped vesicular stomatitis virus (VSV) virus, essentially as described in Sanchez-Felipe et al.[18] Briefly, depending on the plasmid background, BHK-21J cells (for the WA1/2020-like B.1/D614G variant, as described in Sanchez-Felipe et al.[18])

or HEK-293T cells (for the Beta and Delta variants, as sourced from Invivogen cat. nos. plv-spike-v3 and plv-spike-v8, respectively) were transfected with SARS-CoV-2 Spike protein expression plasmids and 1 day later infected with GFP-encoding VSVΔG backbone virus. Two hours later, the medium was replaced by medium containing anti-VSV-G antibody (I1-hybridoma, ATCC CRL-2700) to neutralize residual VSV-G input. After 26 h of incubation at 32°C, the supernatants were harvested. To quantify SARS-CoV-2 NAbs, serial dilutions of serum samples were incubated for 1 h at 37°C with an equal volume of Spike-pseudotyped VSV particles and inoculated on Vero E6 cells for 19 h (10,000 cells/well were seeded 18 h before infection on 96-well plates and incubated at 37°C and 5% of CO_2). The resulting number of GFP-expressing cells was quantified on a Cell Insight CX5 High Content Screening platform (Thermo Fisher Scientific) with Thermo Fisher Scientific HCS Studio (version 6.6.0) software. NT_{50}s were determined by curve fitting in GraphPad Prism (GraphPad, San Diego, CA, USA) after normalization to virus (100%) and cell controls (0%) (inhibitor versus response, variable slope, four parameters model with top and bottom constraints of 100% and 0%, respectively).

Analysis of cell-mediated immune response

Splenocyte isolation and stimulation

Freshly harvested mouse spleens were pressed through a 70-μm cell strainer. The resulting cell solution was collected on ice in RPMI High Glucose (4.5 g/L glucose), supplemented with 1% L-glutamine/100X GlutamaX, 10% FBS, and 1% 100× Penicillin G-sodium streptomycin sulfate (PGS). Cells were centrifuged (350 × *g*, 3 min) and resuspended in 1 mL ACK lysis buffer (5–10 min, RT). After rinsing with complete RPMI and centrifugation (350 × *g*, 5 min), pellets were resuspended in medium and counted via trypan blue staining (1:1) with a Cytosmart cell counter (Corning Life Sciences, Corning, NY, USA). Isolated splenocytes were cultured (1×10^6 cells/well) in 96-well plates and stimulated for 6 h with 2.5 μg/mL 1X peptide mix/mL (Miltenyi Biotec, Bergisch Gladbach, Germany) in RPMI or RPMI alone for negative control. Peptivator S protein SARS-CoV-2 (130-126-700, Miltenyi) and Peptivator N protein SARS-CoV-2 (130-126-698, Miltenyi) were used as S- and N-peptide pools, respectively. After 2 h, 1X Transport inhibition cocktail (TIC, eBioscience™ Protein Transport Inhibitor Cocktail [500X], Thermo Fisher Scientific) was added and cells were further incubated for 4 h.

Flow cytometry and intracellular cytokine staining

Freshly isolated and restimulated splenocytes (1×10^6) were spun down (350 × *g*, 5 min), resuspended in Zombie NIR dye (1:1,000 in PBS, #423106; Biolegend, San Diego, CA, USA), and incubated for 30 min, protected from light, at RT. Next, cells were washed and resuspended in fluorescence-activated cell sorting (FACS) staining buffer (PBS, 4% fetal calf serum [FCS], 5 mM EDTA) up to a volume of 100 μL and stained with 1:50 diluted CD3-FITC (#1002405, Biolegend), CD4-PE (#100408, Biolegend) and CD8 Pacific Blue (#100725, Biolegend) staining antibodies for 20 min, protected from light, at 2°–8°C. Cells were washed and spun down (300 × *g*, 10 min), and pellets were resuspended in staining buffer. For intracellular staining of IFN-γ, the Inside Stain kit (#130-090-477; Miltenyi Biotec) was used following the manufacturer's protocol. In brief, cells were incubated with an equal volume of Inside Fix for 20 min at RT, spun down (600 × *g*, 5 min), resuspended in staining buffer, and spun down again (600 × *g*, 5 min). The pellet was resuspended in 100 μL Inside Perm containing staining antibodies (1:400 IFN-γ and mAb-APC, #505810, Biolegend) and incubated for 10 min at RT, before the addition of 150 μL extra Inside Perm. Cells were centrifuged (600 × *g*, 5 min) and resuspended in 250 μL of staining buffer before data acquisition by flow cytometry. The data were analyzed using CytExpert (Beckman Coulter Life Sciences, Indianapolis, IN, USA). All of the measurements were calculated by subtracting nonstimulated samples from the corresponding stimulated samples.

Cytokine profiling of splenocyte supernatant

Cytokine release in the supernatant from stimulated splenocytes was quantified using the LEGENDplex Mouse Th Cytokine Panel (741,044-100T, Biolegend) according to the manufacturer's guidelines using a V-bottom plate (Thermo Fisher Scientific). In short, 25 μL of vortexed capture beads were incubated with standards and samples on a shaker set at 800 rpm for 2 h at RT (protected from light) and spun down (250 × *g*, 5 min, RT). Beads were washed and incubated with 25 μL detection antibodies on a shaker set at 800 rpm for 1 h at RT (protected from light). An equal amount of streptavidin-phycoerythrin was added and incubated (shaker set at 800 rpm, 30 min, RT, protected from light), and beads were spun down (250 × *g*, 5 min), washed, and resuspended in 150 μL washing buffer before data acquisition using a Cytoflex flow cytometer (Beckman Coulter Life Sciences). The data were processed using Qognit (Qognit USA, accessed through Biolegend), a cloud-based software for analyzing multiplexed bead assays.

qRT-PCR for SARS-CoV-2 viral load and cytokine analysis

Hamster lung tissues were collected after sacrifice and were homogenized using bead disruption (Precellys, Bertin Corp, Rockville, MD, USA) in 350 μL RLT buffer (RNeasy Mini kit, Qiagen) and centrifuged (10,000 rpm, 5 min) to pellet the cell debris. RNA was extracted according to the manufacturer's instructions. Of the 50 μL eluate, 4 μL was used as a template in qRT-PCR reactions. qRT-PCR was performed on a LightCycler96 platform (Roche, Basel, Switzerland) using the iTaq Universal Probes One-Step qRT-PCR kit (BioRad, Hercules, CA, USA) with N2 primers and probes targeting the nucleocapsid as described by Boudewijns et al.[19] Standards of SARS-CoV-2 cDNA (IDT) were used to express viral genome copies per milligram of tissue or per milliliter of serum. Expression levels of IL-6 and IP-10 were normalized to the expression of β-actin. The relative fold change was calculated using the $2^{-\Delta\Delta Ct}$ method.[46] To quantify infectious SARS-CoV-2 particles in the homogenized lung tissues, endpoint titrations were performed on confluent Vero E6 cells in 96-well plates. Viral titers were calculated by the Reed-Muench method[42] using the Lindenbach calculator and were expressed as $TCID_{50}$ per milligram of tissue.

Lung histology

For histological examination, the lungs were fixed overnight in 4% formaldehyde and embedded in paraffin. Tissue sections (5 μm)

were analyzed after staining with hematoxylin and eosin (H&E) and scored blindly for lung damage by an expert pathologist. The 14 scoring parameters, to which a value of 1–3 was attributed, were the following: congestion, intra-alveolar hemorrhage, intra-alveolar edema, lymphoid follicles, apoptotic bodies in bronchus wall, necrotizing bronchiolitis, perivascular edema, bronchopneumonia (and percentage of lungs involved), perivascular inflammation, endothelialitis, perivascular cuffs, peribronchial inflammation, intraluminal polymorphonuclear neutrophil (PMN), and vasculitis. Cumulative lung scores are presented as median.

Statistical analysis

Statistical analyses were performed using GraphPad Prism 9. Normality was analyzed using the D'Agostino and Pearson omnibus test, and assumptions of normality and homoscedasticity were confirmed using graphical methods (visualization via QQ plots). Normally distributed data of two groups were compared via t tests, and multiple groups were compared by one-way analysis of variance (-ANOVA) test and followed by the Holm-Sidak test. Non-normally distributed data were analyzed via Kruskal-Wallis tests with Dunn's correction for multiple comparisons or Mann-Whitney tests for comparison of two groups. Gaussian distributed data are presented as (geometric) mean ± (geometric) SD, non-normally distributed data are presented as median with IQR (unless stated differently in the figure legends). p-values are reported as two-sided and considered significant when less than 0.05 (*$p < 0.05$, **$p < 0.01$, ***$p < 0.001$, ****$p < 0.0001$).

SUPPLEMENTAL INFORMATION

Supplemental information can be found online at https://doi.org/10.1016/j.ymthe.2022.04.014.

ACKNOWLEDGMENTS

The authors want to thank Leonie Wyffels (Ziphius Vaccines NV) for her feedback during the preparation of the manuscript; Dominique Van Looveren, Thomas Vercruysse, and Hendrik Jan Thibaut (Rega Institute for Medical Research Laboratory of Virology and Chemotherapy) for their role in the planning and coordination of the wild-type VNT serology studies; and Delphine Acar for her contribution in the preparation of the human serum samples. This work was supported by the Flanders Innovation & Entrepreneurship (Vlaams Agentschap Innoveren & Ondernemen, VLAIO) Project HBC.2020.2481, which was granted to Ziphius Vaccines NV.

AUTHOR CONTRIBUTIONS

S.M., A.K.M.A.H., I.S., and N.N.S. conceptualized the antigen design and designed the *in vitro* and *in vivo* mouse studies and the data analysis; B.W., M.P., and M.S. aided in performing the *in vitro* and *in vivo* mouse studies; I.S. and N.N.S. coordinated and supervised all of the mouse studies; S.M., A.K.M.A.H., S.V., and I.S. designed and prepared the saRNA and LNP studies; N.F. assisted in performing the LNP studies; S.M., A.K.M.A.H., A.V., and I.S. planned the experimental design for the hamster experiments; R.A. and C.S.F. planned the methodology and performed and analyzed the data of the hamster studies; J.N. coordinated and supervised the hamster studies; L.H., J.M., and K.K.A. conceived of and performed the wild-type viral neutralization assays; K.K.A. coordinated and supervised the wild-type viral neutralization studies; L.V. obtained and provided the human serum samples; A.V. performed the final statistical analysis, drafted the manuscript, and designed the graphs and figures. All of the authors contributed to manuscript editing and provided constructive feedback and final approval.

DECLARATION OF INTEREST

S.M., A.K.M.A.H., A.V., B.W., M.P., M.S., S.V., and I.S. are current employees of Ziphius Vaccines NV and may own Ziphius shares/warrants. S.M., A.K.M.A.H., S.V., I.S., and N.N.S. are inventors on a patent application claiming subject matter related to the SARS-CoV-2 saRNA vaccine candidates described herein. The Virology Unit of the Institute of Tropical Medicine, supervised by K.K.A., and the Department of Microbiology, Immunology, and Transplantation of Rega Institute for Medical Research (KUL), supervised by J.N., received compensation from Ziphius Vaccines NV to perform the neutralization assays and hamster studies, respectively. The authors declare no other competing interests.

REFERENCES

1. Coronavirus Disease (COVID-19). https://www.who.int/emergencies/diseases/novel-coronavirus-2019.
2. Guan, W.J., Ni, Z.Y., Hu, Y., Liang, W.H., Ou, C.Q., He, J.X., Liu, L., Shan, H., Lei, C.L., Hui, D.S.C., et al. (2020). Clinical characteristics of Coronavirus disease 2019 in China. N. Engl. J. Med. *382*, 1708–1720. https://doi.org/10.1056/nejmoa2002032.
3. Machado, B.A.S., Hodel, K.V.S., Fonseca, L.M.d.S., Mascarenhas, L.A.B., Andrade, L.P. C.d.S., Rocha, V.P.C., Soares, M.B.P., Berglund, P., Duthie, M.S., Reed, S.G., et al. (2021). The importance of RNA-based vaccines in the fight against COVID-19: an overview. Vaccines (Basel) *9*, 1345. https://doi.org/10.3390/vaccines9111345.
4. Vogel, A.B., Kanevsky, I., Che, Y., Swanson, K.A., Muik, A., Vormehr, M., Kranz, L.M., Walzer, K.C., Hein, S., Güler, A., et al. (2020). A prefusion SARS-CoV-2 spike RNA vaccine is highly immunogenic and prevents lung infection in non-human primates. Preprint at bioRxiv. https://doi.org/10.1101/2020.09.08.280818.
5. Corbett, K.S., Flynn, B., Foulds, K.E., Francica, J.R., Boyoglu-Barnum, S., Werner, A.P., Flach, B., O'Connell, S., Bock, K.W., Minai, M., et al. (2020). Evaluation of the mRNA-1273 vaccine against SARS-CoV-2 in nonhuman primates. N. Engl. J. Med. *383*, 1544–1555. https://doi.org/10.1056/nejmoa2024671.
6. Blakney, A.K., Ip, S., and Geall, A.J. (2021). An update on self-amplifying mRNA vaccine development. Vaccines (Basel) *9*, 97. https://doi.org/10.3390/vaccines9020097.
7. Shrotri, M., Navaratnam, A.M.D., Nguyen, V., Byrne, T., Geismar, C., Fragaszy, E., Beale, S., Fong, W.L.E., Patel, P., Kovar, J., et al. (2021). Spike-antibody waning after second dose of BNT162b2 or ChAdOx1. Lancet *398*, 385–387. https://doi.org/10.1016/s0140-6736(21)01642-1.
8. Hoffmann, M., Arora, P., Groß, R., Seidel, A., Hornich, B.F., Hahn, A.S., Kruger, N., Graichen, L., Hofmann-Winkler, H., Kempf, A., et al. (2021). SARS-CoV-2 variants B.1.351 and P.1 escape from neutralizing antibodies. Cell *184*, 2384–2393.e12. https://doi.org/10.1016/j.cell.2021.03.036.
9. Goel, R.R., Painter, M.M., Apostolidis, S.A., Mathew, D., Meng, W., Rosenfeld, A.M., Lundgreen, K.A., Reynaldi, A., Khoury, D.S., Pattekar, A., et al.; The UPenn COVID Processing Unit (2021). mRNA vaccines induce durable immune memory to SARS-CoV-2 and variants of concern. Science *374*, abm0829. https://doi.org/10.1126/science.abm0829.
10. Gazit, S., Shlezinger, R., Perez, G., Lotan, R., Peretz, A., Ben-Tov, A., Cohen, D., Muhsen, K., Chodick, G., and Patalon, T. (2021). Comparing SARS-CoV-2 natural immunity to vaccine-induced immunity: reinfections versus breakthrough infections. Preprint at medRxiv. https://doi.org/10.1101/2021.08.24.21262415.

11. Garcia-Beltran, W.F., St Denis, K.J., Hoelzemer, A., Lam, E.C., Nitido, A.D., Sheehan, M.L., Berrios, C., Ofoman, O., Chang, C.C., Hauser, B.M., et al. (2022). mRNA-based COVID-19 vaccine boosters induce neutralizing immunity against SARS-CoV-2 Omicron variant. Cell *185*, 457–466.e4. https://doi.org/10.1016/j.cell.2021.12.033.

12. Xu, K., Dai, L., and Gao, G.F. (2021). Humoral and cellular immunity and the safety of COVID-19 vaccines: a summary of data published by 21 May 2021. Int. Immunol. *33*, 529–540. https://doi.org/10.1093/intimm/dxab061.

13. Wang, Z., Schmidt, F., Weisblum, Y., Muecksch, F., Barnes, C.O., Finkin, S., Schaefer-Babajew, D., Cipolla, M., Gaebler, C., Lieberman, J.A., et al. (2021). mRNA vaccine-elicited antibodies to SARS-CoV-2 and circulating variants. Nature *592*, 616–622. https://doi.org/10.1038/s41586-021-03324-6.

14. Tarke, A., Sidney, J., Kidd, C.K., Dan, J.M., Ramirez, S.I., Yu, E.D., Mateus, J., da Silva Antunes, R., Moore, E., Rubiro, P., et al. (2021). Comprehensive analysis of T cell immunodominance and immunoprevalence of SARS-CoV-2 epitopes in COVID-19 cases. Medicine *2*, 100204. https://doi.org/10.1016/j.xcrm.2021.100204.

15. Dong, Y., Dai, T., Wei, Y., Zhang, L., Zheng, M., and Zhou, F. (2020). A systematic review of SARS-CoV-2 vaccine candidates. Signal Transduct. Target Ther. *5*, 237. https://doi.org/10.1038/s41392-020-00352-y.

16. de Alwis, R., Gan, E.S., Chen, S., Leong, Y.S., Tan, H.C., Zhang, S.L., Yau, C., Low, J.G.H., Kalimuddin, S., Matsuda, D., et al. (2021). A single dose of self-transcribing and replicating RNA-based SARS-CoV-2 vaccine produces protective adaptive immunity in mice. Mol. Ther. *29*, 1970–1983. https://doi.org/10.1016/j.ymthe.2021.04.001.

17. Petrakova, O., Volkova, E., Gorchakov, R., Paessler, S., Kinney, R.M., and Frolov, I. (2005). Noncytopathic replication of Venezuelan equine encephalitis virus and eastern equine encephalitis virus replicons in Mammalian cells. J. Virol. *79*, 7597–7608. https://doi.org/10.1128/jvi.79.12.7597-7608.2005.

18. Sanchez-Felipe, L., Vercruysse, T., Sharma, S., Ma, J., Lemmens, V., Van Looveren, D., Arkalagud Javarappa, M.P., Boudewijns, R., Malengier-Devlies, B., Liesenborghs, L., et al. (2021). A single-dose live-attenuated YF17D-vectored SARS-CoV-2 vaccine candidate. Nature *590*, 320–325. https://doi.org/10.1038/s41586-020-3035-9.

19. Boudewijns, R., Thibaut, H.J., Kaptein, S.J.F., Li, R., Vergote, V., Seldeslachts, L., Van Weyenbergh, J., De Keyzer, C., Bervoets, L., Sharma, S., et al. (2020). STAT2 signaling restricts viral dissemination but drives severe pneumonia in SARS-CoV-2 infected hamsters. Nat. Commun. *11*, 5838. https://doi.org/10.1038/s41467-020-19684-y.

20. Richner, J.M., Himansu, S., Dowd, K.A., Butler, S.L., Salazar, V., Fox, J.M., Julander, J.G., Tang, W.W., Shresta, S., Pierson, T.C., et al. (2017). Modified mRNA vaccines protect against Zika virus infection. Cell *168*, 1114–1125.e10. https://doi.org/10.1016/j.cell.2017.02.017.

21. Bahl, K., Senn, J.J., Yuzhakov, O., Bulychev, A., Brito, L.A., Hassett, K.J., Laska, M.E., Smith, M., Almarsson, O., Thompson, J., et al. (2017). Preclinical and clinical demonstration of immunogenicity by mRNA vaccines against H10N8 and H7N9 Influenza viruses. Mol. Ther. *25*, 1316–1327. https://doi.org/10.1016/j.ymthe.2017.03.035.

22. Alberer, M., Gnad-Vogt, U., Hong, H.S., Mehr, K.T., Backert, L., Finak, G., Gottardo, R., Bica, M.A., Garofano, A., Koch, S.D., et al. (2017). Safety and immunogenicity of a mRNA rabies vaccine in healthy adults: an open-label, non-randomised, prospective, first-in-human phase 1 clinical trial. Lancet *390*, 1511–1520. https://doi.org/10.1016/s0140-6736(17)31665-3.

23. Zhong, Z., Mc Cafferty, S., Combes, F., Huysmans, H., De Temmerman, J., Gitsels, A., Vanrompay, D., Portela Catani, J., and Sanders, N.N. (2018). mRNA therapeutics deliver a hopeful message. Nano Today *23*, 16–39. https://doi.org/10.1016/j.nantod.2018.10.005.

24. Zhong, Z., McCafferty, S., Opsomer, L., Wang, H., Huysmans, H., De Temmerman, J., Lienenklaus, S., Portela Catani, J.P., Combes, F., and Sanders, N.N. (2021). Corticosteroids and cellulose purification improve, respectively, the in vivo translation and vaccination efficacy of sa-mRNAs. Mol. Ther. *29*, 1370–1381. https://doi.org/10.1016/j.ymthe.2021.01.023.

25. Pollock, K.M., Cheeseman, H.M., Szubert, A.J., Libri, V., Boffito, M., Owen, D., Bern, H., O'Hara, J., McKay, P., Rampling, T., et al. (2022). Safety and immunogenicity of a self-amplifying RNA vaccine against COVID-19: COVAC1, a phase I, dose-ranging trial. EClinicalMedicine *44*, 101262. https://doi.org/10.1016/j.eclinm.2021.101262.

26. McKay, P.F., Hu, K., Blakney, A.K., Samnuan, K., Brown, J.C., Penn, R., Zhou, J., Bouton, C.R., Rogers, P., Polra, K., et al. (2020). Self-amplifying RNA SARS-CoV-2 lipid nanoparticle vaccine candidate induces high neutralizing antibody titers in mice. Nat. Commun. *11*, 3523. https://doi.org/10.1038/s41467-020-17409-9.

27. Erasmus, J.H., Khandhar, A.P., O'Connor, M.A., Walls, A.C., Hemann, E.A., Murapa, P., Archer, J., Leventhal, S., Fuller, J.T., Lewis, T.B., et al. (2020). An Alphavirus-derived replicon RNA vaccine induces SARS-CoV-2 neutralizing antibody and T cell responses in mice and nonhuman primates. Sci. Transl. Med. *12*, eabc9396. https://doi.org/10.1126/scitranslmed.abc9396.

28. Rappaport, A.R., Hong, S.-J., Scallan, C.D., Gitlin, L., Akoopie, A., Boucher, G.R., Egorova, M., Espinosa, J.A., Fidanza, M., Kachura, M.A., et al. (2021). A self-amplifying mRNA COVID-19 vaccine drives potent and broad immune responses at low doses that protects non-human primates against SARS-CoV-2. Preprint at bioRxiv. https://doi.org/10.1101/2021.11.08.467773.

29. Spencer, A.J., McKay, P.F., Belij-Rammerstorfer, S., Ulaszewska, M., Bissett, C.D., Hu, K., Samnuan, K., Blakney, A.K., Wright, D., Sharpe, H.R., et al. (2021). Heterologous vaccination regimens with self-amplifying RNA and adenoviral COVID vaccines induce robust immune responses in mice. Nat. Commun. *12*, 2893. https://doi.org/10.1038/s41467-021-23173-1.

30. Maruggi, G., Mallett, C.P., Westerbeck, J.W., Chen, T., Lofano, G., Friedrich, K., Qu, L., Sun, J.T., McAuliffe, J., Kanitkar, A., et al. (2022). A self-amplifying mRNA SARS-CoV-2 vaccine candidate induces safe and robust protective immunity in preclinical models. Mol. Ther. https://doi.org/10.1016/j.ymthe.2022.01.001.

31. Sanders, N.N. (2021). Low-dose single-shot COVID-19 mRNA vaccines lie ahead. Mol. Ther. *29*, 1944–1945. https://doi.org/10.1016/j.ymthe.2021.05.003.

32. Guo, Y., He, W., Mou, H., Zhang, L., Chang, J., Peng, S., Ojha, A., Tavora, R., Parcells, M.S., Luo, G., et al. (2021). An engineered receptor-binding domain improves the immunogenicity of multivalent SARS-CoV-2 vaccines. mBio *12*. e00930–21.

33. Mc Cafferty, S., De Temmerman, J., Kitada, T., Becraft, J.R., Weiss, R., Irvine, D.J., Devreese, M., De Baere, S., Combes, F., and Sanders, N.N. (2021). In vivo validation of a reversible small molecule-based switch for synthetic self-amplifying mRNA regulation. Mol. Ther. *29*, 1164–1173. https://doi.org/10.1016/j.ymthe.2020.11.010.

34. Wroblewska, L., Kitada, T., Endo, K., Siciliano, V., Stillo, B., Saito, H., and Weiss, R. (2015). Mammalian synthetic circuits with RNA binding proteins for RNA-only delivery. Nat. Biotechnol. *33*, 839–841. https://doi.org/10.1038/nbt.3301.

35. Le Bert, N., Tan, A.T., Kunasegaran, K., Tham, C.Y.L., Hafezi, M., Chia, A., Chng, M.H.Y., Lin, M., Tan, N., Linster, M., et al. (2020). SARS-CoV-2-specific T cell immunity in cases of COVID-19 and SARS, and uninfected controls. Nature *584*, 457–462. https://doi.org/10.1038/s41586-020-2550-z.

36. Magini, D., Giovani, C., Mangiavacchi, S., Maccari, S., Cecchi, R., Ulmer, J.B., De Gregorio, E., Geall, A.J., Brazzoli, M., and Bertholet, S. (2016). Self-amplifying mRNA vaccines expressing multiple conserved influenza antigens confer protection against homologous and heterosubtypic viral challenge. PLoS One *11*, e0161193. https://doi.org/10.1371/journal.pone.0161193.

37. Grifoni, A., Weiskopf, D., Ramirez, S.I., Mateus, J., Dan, J.M., Moderbacher, C.R., Rawlings, S.A., Sutherland, A., Premkumar, L., Jadi, R.S., et al. (2020). Targets of T Cell responses to SARS-CoV-2 Coronavirus in humans with COVID-19 disease and unexposed individuals. Cell *181*, 1489–1501.e15. https://doi.org/10.1016/j.cell.2020.05.015.

38. DiPiazza, A.T., Graham, B.S., and Ruckwardt, T.J. (2021). T cell immunity to SARS-CoV-2 following natural infection and vaccination. Biochem. Biophys. Res. Commun. *538*, 211–217. https://doi.org/10.1016/j.bbrc.2020.10.060.

39. WHO Global Consultation - what evidence do we have that omicron is evading immunity and what are the implications?. https://www.who.int/news-room/events/detail/2021/12/15/default-calendar/who-global-consultation—what-evidence-do-we-have-that-omicron-is-evading-immunity-and-what-are-the-implications.

40. Baiersdorfer, M., Boros, G., Muramatsu, H., Mahiny, A., Vlatkovic, I., Sahin, U., and Kariko, K. (2019). A facile method for the removal of dsRNA contaminant from in vitro-transcribed mRNA. Mol. Ther. Nucleic Acids *15*, 26–35. https://doi.org/10.1016/j.omtn.2019.02.018.

41. Geall, A.J., Verma, A., Otten, G.R., Shaw, C.A., Hekele, A., Banerjee, K., Cu, Y., Beard, C.W., Brito, L.A., Krucker, T., et al. (2012). Nonviral delivery of self-amplifying RNA

vaccines. Proc. Natl. Acad. Sci. U S A *109*, 14604–14609. https://doi.org/10.1073/pnas.1209367109.

42. Reed, L.J., and Muench, H. (1938). A simple method of estimating fifty per cent endpoints. Am. J. Epidemiol. *27*, 493–497. https://doi.org/10.1093/oxfordjournals.aje.a118408.

43. Geisinger, J.M., Turan, S., Hernandez, S., Spector, L.P., and Calos, M.P. (2016). In vivo blunt-end cloning through CRISPR/Cas9-facilitated non-homologous end-joining. Nucleic Acids Res. *44*, e76. https://doi.org/10.1093/nar/gkv1542.

44. Pannus, P., Neven, K.Y., De Craeye, S., Heyndrickx, L., Vande Kerckhove, S., Georges, D., Michiels, J., Francotte, A., Van Den Bulcke, M., Zrein, M., et al. (2021). Poor antibody response to BioNTech/Pfizer COVID-19 vaccination in SARS-CoV-2 naive residents of nursing homes. Clin. Infect. Dis. ciab998.

45. Marien, J., Ceulemans, A., Michiels, J., Heyndrickx, L., Kerkhof, K., Foque, N., Widdowson, M.A., Mortgat, L., Duysburgh, E., Desombere, I., et al. (2021). Evaluating SARS-CoV-2 spike and nucleocapsid proteins as targets for antibody detection in severe and mild COVID-19 cases using a Luminex bead-based assay. J. Virol. Methods *288*, 114025. https://doi.org/10.1016/j.jviromet.2020.114025.

46. Livak, K.J., and Schmittgen, T.D. (2001). Analysis of relative gene expression data using real-time quantitative PCR and the $2-\Delta\Delta CT$ method. Methods *25*, 402–408. https://doi.org/10.1006/meth.2001.1262.